Slutrapport
Energieffektiva fartyg med luftkammare

Energimyndigheten, projektnummer 34047-1

Rickard Bensow
Sjöfart och marin teknik
Chalmers tekniska högskola

1 Introduktion

Denna rapport beskriver arbetet utfört i projektet Energieffektiva fartyg med luftkammare, projektnummer 34047-1, delvis med ett överlapp med tidigare lägesrapport 1 och 2. Projektet har löpt under drygt två år med finansiering från Energimyndigheten (50%) och Stena AB (50%) avseende forskningsarbete och försök på både Chalmers tekniska högskola (Inst. Sjöfart och Marin teknik) och SSPA AB. Syftet med projektet har varit att undersöka tekniken med att nyttja en trycksatt luftkammare i botten på ett deplacerande fartyg för att reducera motståndet mellan skrovet och vattnet och därmed minska energibehovet för fartygets framdrivning.
Målsättningarna var att

1. Nå en bättre förståelse för strömningsfenomenen i och kring luftkammaren, för att därigenom
2. Försöka applicera denna ökade kunskapsnivå för att förbättra funktionen av luftkammaren, d.v.s. minska fartygets motstånd ytterligare och komma närmare de teoretiskt ideala minskningarna, samt att
3. Föra över denna kunskap till avnämare inom näringen så att projektets resultat potentiellt kan realiseras på ett fartyg i kommersiell trafik.

En ytterligare positiv bi-effekt som projektet avsåg att leda till var ett utökat samarbete mellan Stena, SSPA, och Chalmers, vilka alla tre är viktiga aktörer inom svensk sjöfartsnäring och –industri.
De ovan nämnda målsättningarna har i stort uppfyllts, även om vi inte nått tillräckligt långt för att lösningen ska vara tillräckligt fördelaktig för att direkt utvecklas för kommersiell trafik med nuvarande bränslekostnader. Sammanfattningsvis har vi

1. En väsentligt bättre kunskap kring vilka förlustkomponenter som gör att resultaten avviker från ideal motståndsminskning;
2. Utvecklat och testat en konstruktionsförändring som förbättrat resultatet något, men framför allt har gjort beteendet mer robust relativt driftskonditioner;
3. Genom frekventa och regelbundna möten mellan alla tre involverade partners tillgodosett att näringen har haft god insyn i projektets utförande och resultat och kunnat ge värdefull feedback och styrning mot relevanta frågeställningar.

Rapporten inleds med en kort bakgrund till tekniken med luftkammare, varefter projektets organisation, målsättningar och genomförande beskrivs. Därefter ges en kort sammanfattning av de mest intressanta forskningsresultaten, medan en mer komplett redogörelse för resultaten ges som bilagor, både i form av en publikation baserad på projektresultat och, för de resultat som ännu inte publicerats, som kortfattade utdrag ur interna tekniska rapporter.

2 Bakgrund

För långsamt stävande fartyg, såsom de flesta tank- och bulkfartyg, står friktionsmotståndet ofta för runt 80% av det totala motståndet. Att minska detta motstånd för att förbättra energieffektiviteten hos enheten är dock inte rättframt då skrovytan i allmänhet inte är möjlig att minska utan att minska fartygets deplacement och därmed även dess lastkapacitet. En gammal idé, men som tidigare inte varit praktiskt realiserbar, rör att "smörja" med luft över en del av skrovet och därigenom minska den del av skrovytan som är i direkt kontakt med vattnet. Det ökande intresset för resurssnåla och miljövänliga transporter i kombination tekniska framsteg har gjort att denna idé återigen har undersökts av ett flertal parter världen över. Idén med luftsmörjning togs också upp i den STEM-finansierade Chalmersrapporten nr 09:115, "Energy efficiency in shipping" skriven av Lasseson and Andersson, som en teknik med stor besparingspotential.

Det finns flera olika angreppssätt kring luftsmörjning, och i Sverige har Stena Rederi AB tillsammans med SSPA Sweden AB undersökt en teknik som internationellt betecknas som Air Cavity Ships, förkortat ACS, där en stor del av skrovets platta bottenarea ersätts med en luftkudde. Man bygger då skrovet med en hålighet i botten, en kavitet, som fylls med trycksatt luft och idealt ersätter skrovytan; kavitet och luftkudde kommer vidare i rapporten bägge två att användas för att beteckna samma sak. Notera att trycket inte behöver vara särskilt stort och om konstruktionen fungerar som avsett ska ingen luft sippra ut ur kaviteten och arbetet att upprättahålla trycket är litet. Ett större tankfartyg har en relativt stor platt bottenarea och låg fart och är därför en lämplig kandidat för att byggas som ACS. Uppskattningsvis skulle ett skrov kunna ritas med ca 35% bottenyta som kan ersättas med luftkudde som idealt betraktas som friktionslöst vilket potentiellt skulle ge knappt 30% i minskat friktionsmotstånd; baserat på projektresultat vet vi nu att ytterligare förluster som inte går att undvika sänker denna siffra något till, säg, 25%.

Försök har tidigare gjorts i SSPA:s släpränna och även en 15 meter lång demonstrator, Stena Airmax, har byggts och använts för datainsamling under körning till havs i Gullmarsfjorden. Tekniken har visat sig lovande men man har också kunnat konstatera att det finns förluster som inte kunnat förklaras genom de studier som genomförts; systemet med dess vatten/luft-gräns under fartyget är svårt att mäta i detalj.

Detta projekt skapades för att försöka utreda dessa förluster och ge förslag på hur dessa kan motverkas och därigenom också ge ett bättre perspektiv på hur nära den ovan nämnda 30% motståndsminskningen det är realistiskt att förvänta sig att det går att komma.

3 Projektets genomförande

3.1 Frågeställningar

Konceptet med Air Cavity Ship har tidigare prövats när det gäller inlandstrafik eller mindre höghastighetsfartyg och inte för större oceangående deplacerande fartyg som varit i fokus i detta projekt. Nyligen utförda prov, utöver det ovan nämnda arbetet av Stena och SSPA, inkluderar ett koncept av DK group och en inlandspråm av PELS-konsortiet, vilket är ett EU-finansierat forskningsprojekt med MARIN och DST som huvudaktörer. Ett alternativt luftsmörjningssystem finns utvecklat till prototyp, där bubblor används istället för en luftkammare, av bl.a. Mitsubishi Heavy Industries. Publikationer, och därmed även forskningsinsatser, som behandlar ACS är ännu så länge begränsade. Ett antal artiklar har dock publicerats i vetenskapliga tidskrifter och berör då ACS för höghastighetsfartyg eller fartyg i inlandstrafik samt ytterligare ett fåtal som studerat tekniken ur ett mer grundläggande, generiskt perspektiv.
Tidigare studier av Stena och SSPA indikerar möjligheter till en substantiell minskning i motstånd, men också att det finns ett flertal hydrodynamiska fenomen som varken är väl beskrivna eller förstådda. De är inte heller möjliga att studera med tidigare genomförda experimentella studier p.g.a. det komplexa strömningsfallet och gränsytan mellan luft och vatten. Bättre kunskap kring dessa frågeställningar bedömdes därför kunna förbättra konceptet med ACS. Det rörde sig om främst tre områden som sågs som de primära:

- I gränsytan mellan luften i kammaren och vattnet bildas ett vågmönster vars effekt på motståndet har var svårbedömt.
- Detaljer kring vad som händer vid kavitetens avslutning; det gäller både i luften och i vattnet.
- Vad händer när nuvarande skalförsök appliceras vid fullskala; detta rör både hur motståndskomponenter skalar och hur konceptet ska utformas.

Sammanfattningsvis kan vi se att den andra punkten har stor betydelse för konceptets framgång, då hur kaviteten avslutas och hur strömningen beter sig över skrovet akter om kaviteten kan bidra till ett stort extra motstånd som reducerar effekten av luftkammaren. Första punkten har mindre genomslag i den meningen att det inte bidrar direkt till en förlust, men vågmönstret har stor betydelse för hur gränsytan sluts i aktra delen av kaviteten samt i hur stor våt yta man får på sidoväggarna av kaviteten. När det gäller tredje punkten så ser vi att det saknas en del studier kring skaleffekter kring strömningen kring avslutet, återigen, men att de bör vara av mindre betydelse i en projektering av ett fullskalefartyg.

3.2 Projektaktiviteter

Forskningen har bedrivits främst genom en post-doc-forskare som arbetat heltid i projektet, med anställning både på Chalmers och på SSPA. Styrning och kunskapsöverfö-

ring har skett genom månatliga möten med representanter från alla tre parter, inklusive post-doc:n, där både presentation av nya resultat, upplägg av (del)studier och omvärldsanalys har diskuterats. Organisationen har fungerat tillfredsställande och säkerställt en god akademisk höjd på studierna, god relevans vad avser framtida kommersiellt nyttjande och en kontinuerlig kunskapsöverföring till industrin.
Forskningsmetodiken har baserats på teoretiska modeller, datorsimuleringar och experimentella försök i både kavitationstunnel och släpränna. Simuleringar har använts som stöd dels för att designa experimenten och dels för att underlätta tolkningen av resultaten. I det förberedande skedet har det rört sig om att finna lämplig geometrisk utformning och lämpliga konditioner för försöken samt att utvärdera vad som ska mätas, var och hur. I analysskedet har simuleringsresultaten använts för att ge kompletterande information om strömningsfältet och motståndskomponenter som inte har kunnat mätas av diverse begränsningar i mätteknik och –uppställning. Det rör sig t.ex. om att alla delar i en luftkammare inte kan isoleras experimentellt för individuell kraftmätning, detaljer i strömningsfältet då mättekniker för hastighetsfältet inte är tillämpbara i ett dylikt multifassystem, eller analys av rörelsemängdsförluster. Det ska nämnas att det även har varit ett delmål i sig att utveckla en simuleringsmetodik med tillförlitlighet att rangordna olika ACS.
Experiment har gjorts i två omgångar. I första skedet designades och testades en generisk kavitet för experiment i kavitationstunnel, där, jämfört med tidigare försök i släpränna, mer detaljerade kraftmätningar och bättre visuell access var möjlig. Den ökade kunskap kring konceptet som då genererades, tillsammans med simuleringarna, försöktes sedan omsättas i en designförändring som i en andra försöksomgång i släpränna jämfördes med den tidigare designen. Under detta försök gjordes också körningar i vågor för att testa ACS:s rubusthet och effekten av ett varierat tryckfält kring skrovet.

3.3 Rapportering

Rapportering har skett, förutom de kontinuerliga diskussioner som först mellan alla tre projektdeltagande parterna, genom interna rapporter om genomförda försök och simuleringar, genom lägesrapporter till Energimyndigheten, till den vetenskapliga gemenskapen genom konferensdeltagande (presentationer och artiklar) och till allmänheten genom seminarier och inslag i media. Exempel på de senare är ett bidrag till den ansedda Symposium on Naval hydrodynamics (29:de upplagan, augusti 2012 i Göteborg; se bilaga i lägesrapport 2 till Energimyndigheten), presentation vid Transporteffektivitetsdagarna (Chalmers, 2012), samt intervju för SR Vetenskapsradio (kortare inslag onsdag 12/6 2013 och längre reportage om energieffektivisering för fartyg under hösten 2013). Minst en tidskriftsartikel för vetenskaplig publikation är planerad.

4 Resultat

Denna sektion avser endast belysa de huvudsakliga dragen bland framtagna resultat. Mer detaljer ges i rapportens två bilagor där den ena utgörs av en artikel presenterad vid en vetenskaplig konferens (även bifogad lägesrapport 2 men inkluderad här för att göra denna rapport komplett); denna bilaga sammanfattar väl vad som gjordes under första halvan av projektet. Den andra är ett utdrag ur internrapporter med figurer och viss förklarande text som presenterar ännu icke publicerade resultat ur projektets andra halva; att endast utdrag presenteras på detta sätt är för att skydda IP som är inkluderat i de fulla rapporterna.

Experimentserie I/Motståndskomponenter

Första delen av projektet syftade till att skapa ökad kunskap om orsaker till att ideal motståndsminskning inte noterats i tidigare försök, och därmed också skapa förutsättningar för att förbättra prestanda. För detta ändamål skapades därför en isolerad kavitet i en plan platta så att den komplicerade strömningen kring skrovet kunde undvikas, se figur 4 i Bilaga 1 för en schematisk skiss. Denna konfiguration har sedan analyserats både genom datorsimuleringar (CFD, Computational Fluid Dynamics) och genom experiment i SSPA:s kavitationstunnel. Kavitetens geometri varierades genom att djupet och lutningen på bakplattan som avslutar kaviteten ändrades. Driftskonditioner har varierats genom att anströmningshastigheten ändrats, vilket emulerar olika fartygsfarter i fullskala, samt genom att det relativa trycket mellan luftkudden och det yttre hydrostatiska trycket ändrats. Vid försöken mättes krafter på kaviteten, den plana plattan framför kaviteten och den plana plattan efter kaviteten, trycket i ett antal punkter inne i kaviteten, samt luftflöde in i kaviteten; gränsytan luft/vatten dokumenterades också visuellt genom fotografering och videofilmning. Mätningar har också genomförts med kaviteten igensatt för att generera referensvärden. Genom kompletterande CFD-beräkningar har mer detaljerad kraftanalys kunnat genomföras.
Resultaten visar på att det framför allt är tre effekter som ger ett motstånd då kaviteten är i drift. Den första är att då ett vågmönster skapas inne i kaviteten kommer delar av sidoväggarna att komma i kontakt med vatten och denna yta bidrar därmed till fartygets våta yta. Den andra, och dominerande, effekten är att då vattnet träffar avslutningsplattan ger detta upphov till en tryckkraft som bidrar till motståndet; även den våta ytan ökar men detta är en mindre effekt. Slutligen så kommer energiförluster att uppstå då det viskösa gränsskiktet ska återuppbyggas akter om kaviteten; detta kommer sig av att då vattnet under kaviteten upplever en (i princip) friktionslös yta gentemot luften kommer den att återigen möta en skrovyta med friktion efter kaviteten och vi får då vad vi kan kalla en rörelsemängdsförlust när de viskösa effekterna återigen ändrar strömningsbilden.

Tabellen nedan sammanfattar uppskattade och uppmätta motståndskrafter på de olika delarna av kaviteten. För den våta ytan har Schlichtings (McGraw-Hill, 1979) formel använts,

$$C_f = \frac{0.455}{(\log Re)^{2.58}} - \frac{1700}{Re},$$

vilken visade sig ge god överrensstämmelse med experimenten. Den tillkommande våta ytarean har uppskattats från experimentella bilder. Vi kan se att i detta fallet är kaviteten relativt effektiv med en motståndsminskning på 50% (19,4 N istället för 38,88) där det ideala, baserat på minskad våt yta, är 80%. Skillnaden mot det ideala beror på ökad våt yta på sidoväggarna (ca 3%), tryck- och friktionskrafter på avslutningsplattan (ca 21%), samt ett ökat motstånd på akterplattan (om ca 7%) beroende av återstarten av gränsskiktet. De första två är helt avhängigt kavitetens geometri (relativt gränsytan mellan luft och vatten) och kan därmed åtminstone delvis förväntas gå att förbättra genom designförändringar; den sistnämnda är det svårare att se hur man kan undvika och vi har i dagsläget ingen god uppfattning om hur den förändras med skala.

Tabell 1: Uppskattade krafter på enkel kavitet

	Kraft [N]	
Total, utan kavitet		38,88
Platta, utan kavitet	31,26	
Akterplatta, utan kavitet	7,62	
Totalt, med kavitet		19,4
Kavitet, totalt	9,2	
Kavitet, sidoväggar	1,1	
Kavitet, avslutningsplatta	8,1	
Akterplatta, med kavitet	10.2	

Övriga slutsatser baserat på denna del av projektet är att beteendet kring kavitetens avslut är i hög grad avhängigt fartygets fart, då vågmönstret som bildas på ytan i kaviteten är fartberoende, och strömningsbilden förändras kraftigt om kavitetens avslut ligger i en vågdal kontra en vågtopp. Det kunde också konstateras att tryckskillnaden mellan trycket i kaviteten och det hydrostatiska trycket påverkar vågamplituden, där en liten tryckskillnad ger mindre vågor. Detta är i princip önskvärt men ger ett väldigt instabilt beteende med frekventa kraftiga luftutsläpp.

”Nedsänkt” kavitet

Det vidare arbetet fokuserades på att finna möjligheter att minska vågamplituden i kaviteten för att därigenom skapa mer robusta förhållanden med potential till förbättrad utformning av kaviteten, framför allt dess avslutning. Den lösning som valdes att studera vidare är baserad på ett teoretiskt arbete (Schmidt, *Journal of Ship Research*,

Vol. 254, 1981) för fartyg med torr akterspegel, där skrovformens inverkan på häckvågen analyserades. Överfört till ACS innebär det att istället för en skarp kant mellan skrovet uppströms och kavitetens start görs en krökt nedsänkning av skrovet precis för om kaviteten; vi refererar till de två utformningarna som ”skarp” respektive ”nedsänkt” kavitet framöver. Initiala simuleringar med den nedsänkta kaviteten ger en kraftigt minskad amplitud på vågmönstret inne i kaviteten och en mer robust avslutning i kavitetens bakkant, vilket var målsättningen. När det gäller kvantitativa jämförelser avseende motstånd ses dock ingen signifikant skillnad, men det ska då noteras att kaviteten i övrigt är identisk med förväntad potential att kunna förbättras under dessa förändrade betingelser både vad gäller avslutet och minskad våtyta på sidorna av kaviteten.

Experimentserie II/Släprännan

I en ny experimentserie jämfördes prestanda mellan den skarpa kaviteten och den nedsänkta genom släpförsök hos SSPA; dessa genomfördes både i stilla vatten och i måttliga vågor. Beteende i vågor har tidigare inte testats i kontrollerade laboratorieförsök utan har bara skett vid körningar med demonstratormodellen i havet. Experimenten visade att i de testade vågförhållandena påverkade kaviteten signifikant endast i vågor med en våglängd jämförbar med fartygets längd; måttliga vågor innebär här att vi antar att fartyget inte rör sig p.g.a. inkommande vågor, maximalt motsvarande sea state 3 för nordatlanten. Beträffande uppförandet av modellen med nedsänkt kavitet, går det att överföra ovan nämnda erfarenheter från simuleringarna till försöken, d.v.s. vågmönstret i kaviteten är kraftigt reducerat och avslutningen mindre fartberoende. Motståndsmätningarna är dock inte konklusiva utan i vissa förhållanden erhölls ett minskat motstånd medan i andra konditioner var motståndet istället högre. Försök gjordes också med en större kavitet vilket inte bara minskade motståndet utan även förbättrade konsekvensen i resultaten.

Inverkan av skrovform/utvärdering av tillförlitligheten hos CFD

Slutligen har även inverkan av skrovformen undersökts, inom ramen för detta projekt enbart med CFD men gamla experimentresultat har funnits som referens. Bakgrunden till denna delstudie är att i tidigare arbete utvecklades och testades en serie skrovvariationer och, av olika anledningar, valdes den s.k. version 5 ut för fortsatta studier genom demonstratormodellen och denna har även nyttjats i detta projekt. Det fanns dock en kandidat, version 6, med bättre prestanda i modellförsöken. Vi ville nu undersöka om den framtagna CFD metodiken kunde prediktera denna prestandaskillnad och därigenom ge en möjlighet att analysera orsakerna till skillnaden.
Beräkningarna genomfördes under något förenklade förhållanden för att minska beräkningstiden och därigenom möjliggöra att de kunde göras inom ramen för projektet. Havsytan, och därmed fartygsgenererade vågor, negligerades utan strömningen antogs vara symmetrisk kring den stilla vattenytan. Detta påverkar både motståndet direkt,

genom att vågmotståndet inte inkluderas i beräkningen, men också genom att tryckvariationer längs skrovsidan inte blir korrekt predikterade vilket indirekt påverkar kaviteten; detta senare är svårt att uppskatta effekten av.
Resultaten visar på att motståndet vid intakt skrov, d.v.s. utan luftkudde, är nära på identiskt mellan de två skrovvarianterna, vilket också var fallet i de tidigare försöken, och att simuleringarna underpredikterade motståndet med ca 10%, vilket är rimligt med hänsyn till att vågmotståndet inte är inkluderat. När det gäller fallen med kavitet underpredikterades motståndet än mer (med ytterligare 10-15%), men den uppmätta skillnaden i motstånd mellan de två skrovvarianterna kunde predikteras relativt väl och rangordningen mellan versionerna var korrekt. Delstudien visar både på potential och brister i simuleringstekniken att arbeta vidare med, dels med avseende på att nyttja verktyget i designarbete men framför allt för att kunna studera de detaljer i strömningsfysiken som ligger bakom den stora skillnaden mellan de två skrovvarianterna.

5 Slutsatser

Projektresultaten har överlag uppnått de målsättningar som sattes upp, även om tekniken med luftkuddar inte har kunnat utvecklas till att bli moget för kommersiellt nyttjande än. Dock har vi idag betydligt bättre kunskap om orsakerna bakom diskrepansen mellan tidigare försöksresultat och den ideala minskningen; däri ligger också en förbättrad uppfattning om vad en realistisk förväntning på motståndsminskning är. Vi saknar dock samband och förståelse för hur strömningen kring kavitetens avslutning kommer att bete sig i fullskala, vilket är en viktig komponent i ett projekterings- och designarbete.

Den ökade förståelsen för kavitetens motstånd är också en förutsättning för att systematiskt kunna arbeta med designförändringar för att kunna uppnå både högre verkningsgrad och robusthet med konceptet. Här har vi också visat på att CFD, datorsimuleringar av strömningen kring skrovet och i kaviteten, har en god potential och mognadsgrad att kunna stötta ett sådant designarbete.

Framtida utmaningar och forskningsfrågor rör dels ovan nämnda skaleffekter kring anslutningen, som förefaller saknas i litteraturen, men kanske i första hand att utreda vad som gör att det skiljer i prestanda mellan de två i slutskedet testade skrovvarianterna. En ytterligare faktor att studera är strömningen nedströms kaviteten, där potentialen att minska energiförluster vid omstarten av det viskösa gränsskiktet bör studeras; t.ex. kan det möjligen vara värt att försöka ha kontrollerat luftutsläpp? Det är också av stor betydelse att i framtiden studera hur propulsionssystemet påverkas av närvaron av luftkudden.

Bilaga 1

Utdrag ur intern teknisk rapportering avseende projektmånader 15-30.

PREFACE

This appendix contains extracts from internal reports produced in the Swedish Energy Agency project "Energy Efficient Air Cavity Ships," grant no 34047-1; the original reports can not be freely released in order to protect partner IP. The presented results stem from the second half of the project, while research preformed during the first part of the project are well reported in the paper "Hydrodynamics of a Displacement Air Cavity Ship", presented at the 29th Symposium on Naval Hydrodynamics, Göteborg, 26-31 Aug. 2012. The work contain:

- More simulations were performed with two-dimensional flow of the pressurized cavity in water tunnel. Effect of velocity, pressure and beach slope on a wider range of parameters was tested.
- The idea of pre-conditioned inflow, by using a recessed edge before the cavity, was tested through performing 2-D and 3-D simulations.
- We studied the effect of air cavity under a hull by performing a series of resistance measurements in towing tank experimental facility of SSPA. Also the performance of the cavity with the recessed edge in calm water and head wave was studied.
- Computational simulations on two different hull forms with and without pressurized air cavity was performed to study the effect of hull form on cavity performance.

1 Two-dimensional Simulations

1.1 Water velocity effect

Five different 2-D cases with similar boundary conditions were simulated using different water inlet velocity. The case description is given in the table below:

Table 1 - 2D Simulation cases with different velocity.

Case	Water Velocity (m/s)	Cavity Pressure (pa)	Beach slope	Cavity height (mm)
ACS77	1.0	-200	18.4°	100
ACS79	1.5	-200	18.4°	100
ACS75	1.8	-200	18.4°	100
ACS78	1.9	-200	18.4°	100
ACS71	1.96	-200	18.4°	100

The free surface height inside the cavity is compared in the graph below:

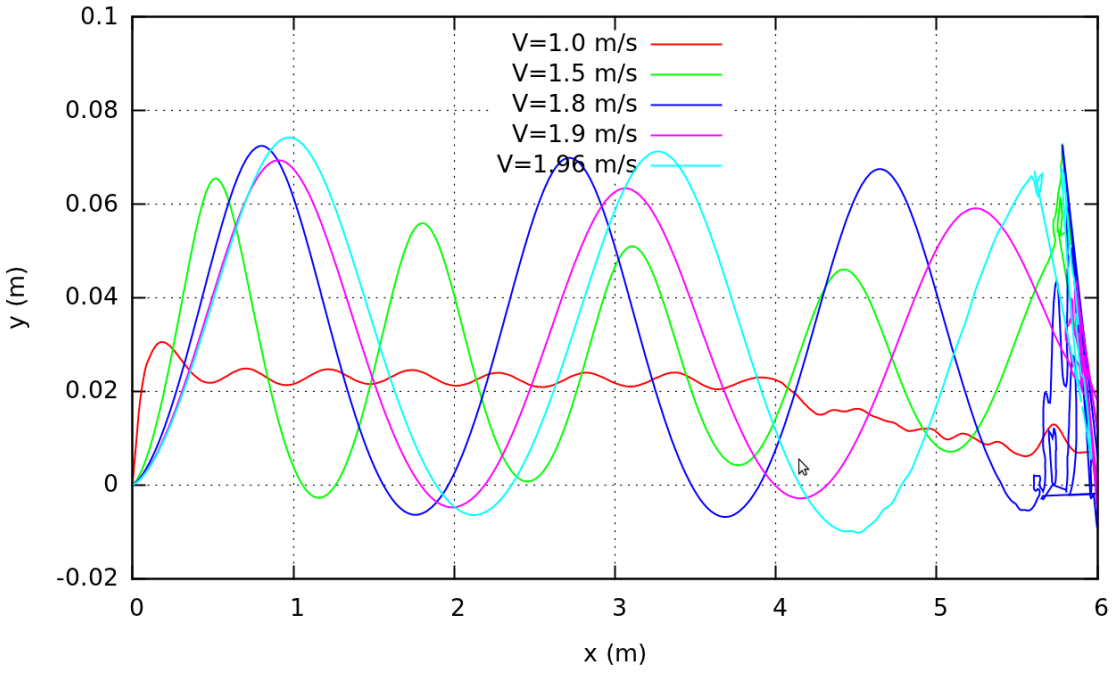

Figure 1 - 2D Simulation free surface elevation in different velocity.

Theoretical values of the wavelength in each case are presented below:

$$\lambda = \frac{2\pi V^2}{g} = (0.8\,V)^2$$

V = 1.0 m/s	→	λ = 0.64 m	→	L/λ = 9.37
V = 1.5 m/s	→	λ = 1.44 m	→	L/λ = 4.16
V = 1.8 m/s	→	λ = 2.08 m	→	L/λ = 2.89
V = 1.9 m/s	→	λ = 2.31 m	→	L/λ = 2.60
V = 1.96 m/s	→	λ = 2.46 m	→	L/λ = 2.44

Compared to the computed values, the number of waves per cavity length are similar in theory and computation of the free surface wave.

The beach re-attachment comparison between these cases is presented as below:

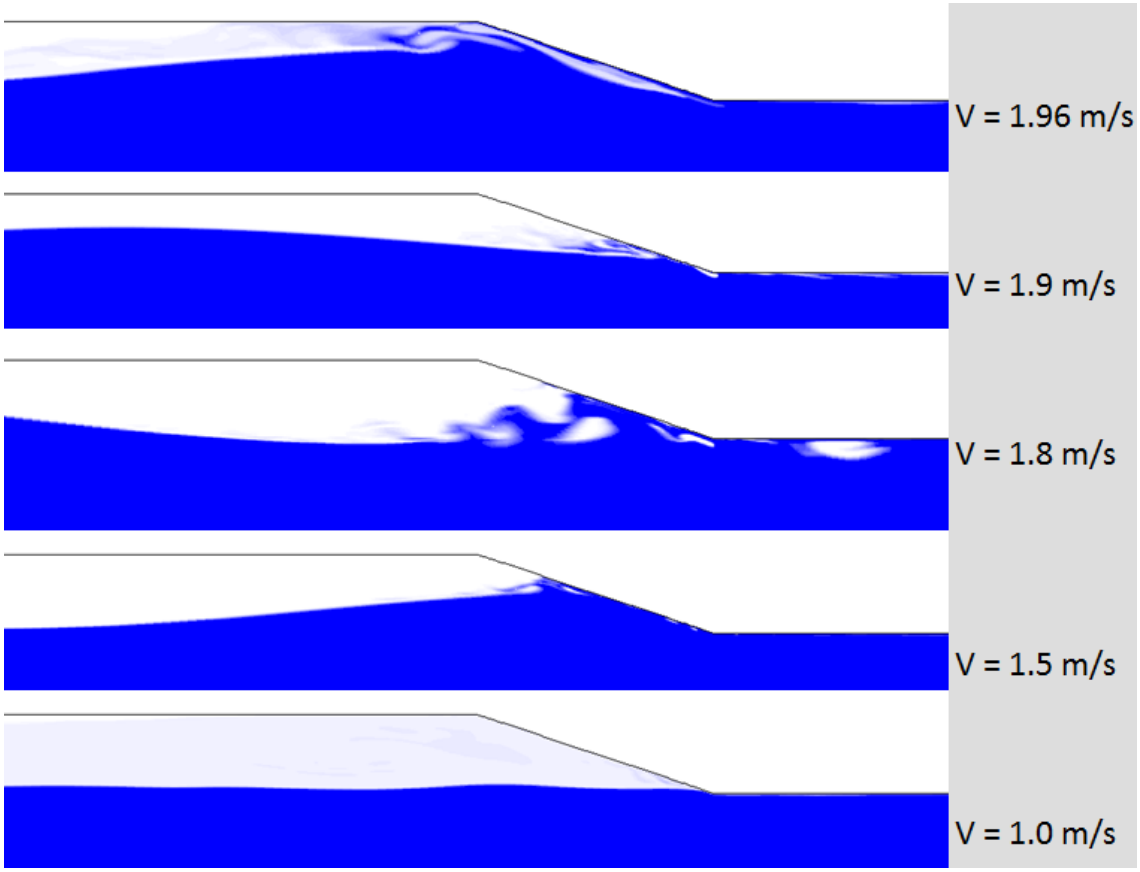

Figure 2 - 2D Simulation, beach re-attachment angle in different velocity.

The picture shows different re-attachment processes with different angles towards the beach. The re-attachment angle depends on the wavelength to cavity length ratio and represents the severity of the pressure force on the beach surface. Since other parameters are constant, the sensitivity of the forces to the velocity can be concluded from these simulations.

The air flow rate into the cavity is compared in different velocities:

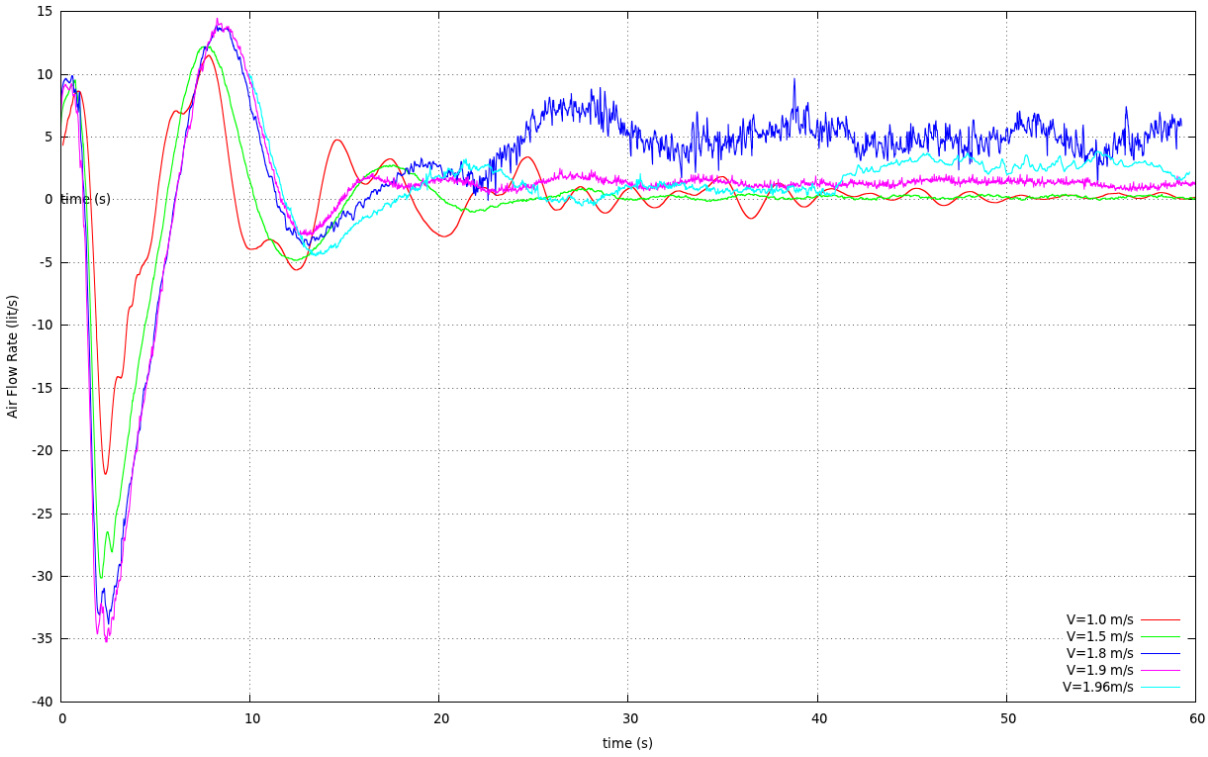

Figure 3 - 2D Simulation, Air flow rate into the cavity in different velocity.

The average values of air flow rate for the last 10 seconds of the run are:

Table 2 - 2D Simulation; Average Air flow rate in different velocity.

Velocity (m/s)	1.0	1.5	1.8	1.9	1.96
Air Flow Rate (lit/s)	0.25	0.22	4.97	1.24	2.72

The average forces acting on different parts for the last 10 seconds are given in the table below:

Table 3 - 2D Simulation; Forces on different parts of the air cavity in different water velocity.

Velocity	Aft Plate	Beach Plate	Fore Plate	Total	Flat plate
1.0 m/s	1.42 N	8.81 N	3.43 N	13.66 N	13.82 N
1.5	3.23	7.40	7.05	17.68	29.7
1.8	1.28	5.02	9.85	16.15	41.9
1.9	1.7	8.24	10.9	20.83	46.3
1.96	3.32	16.07	11.54	30.93	49.1

Different parts of the simulation domain are defined in the picture below:

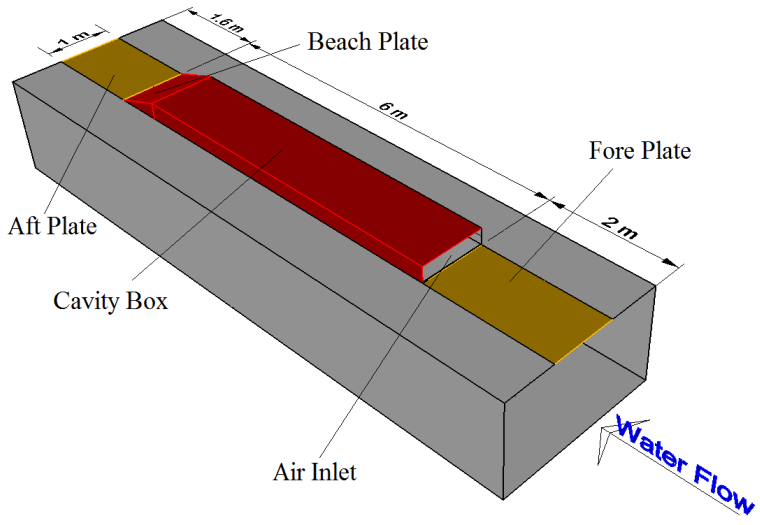

Figure 4 - Schematic of the Air Cavity and test section.

The flat plate theoretical value presented in this table is calculated according to Schlichting 1960 estimation of the coefficient of total skin friction on a flat plate (including Fore and Aft plates):

$$C_f = \frac{0.455}{(\log Re)^{2.58}} - \frac{1700}{Re}$$

1.2 Pressure effect

Three different 2-D cases with similar boundary conditions were compared using different cavity pressures. The case description is given in the table below:

Table 4- 2D Simulation cases with different pressure.

Case	Water Velocity (m/s)	Cavity Pressure (pa)	Beach slope	Cavity height (mm)
ACS71	1.96	-200	18.4°	100
ACS74	1.96	-100	18.4°	100
ACS81	1.96	0	18.4°	100

The free surface height inside the cavity is compared in the graph below:

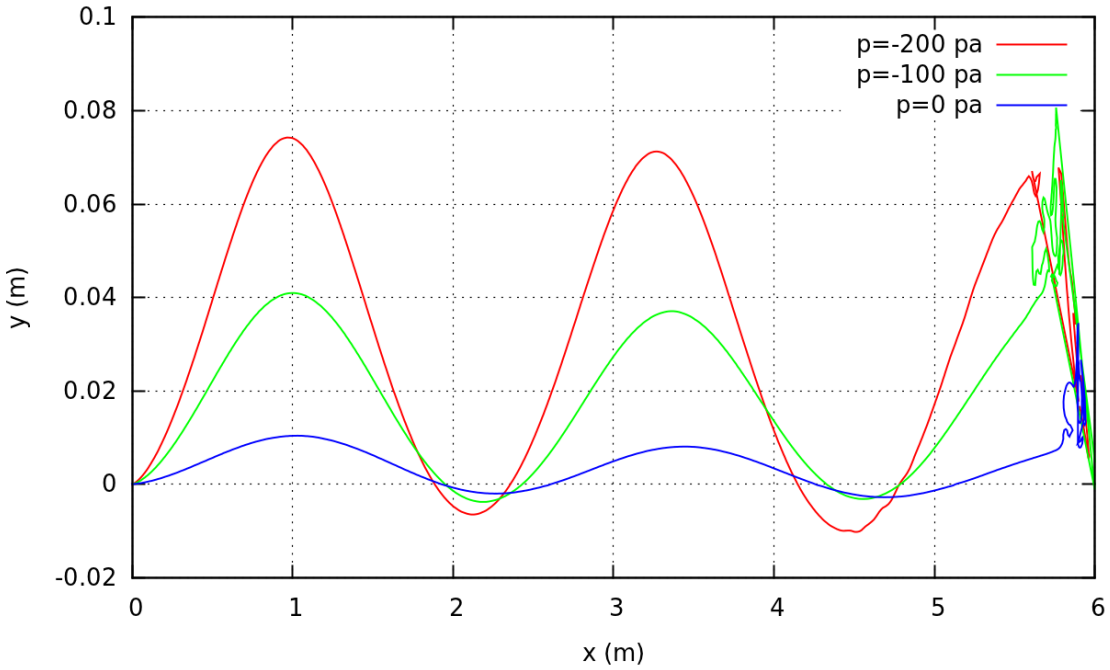

Figure 5 - 2D Simulation free surface elevation in different pressure.

As expected the pressure inside the cavity affects only the amplitude of the wave but does not change the wavelength. Although eventually it changes the position in which the free surface attaches on the beach plate since the beach plate is inclined at the end of cavity.

The beach re-attachment comparison between these cases is presented as below:

Figure 6 - 2D Simulation, beach re-attachment angle in different pressure.

As it is expected, the higher pressure in the case ACS81 has flatter free surface and less force acting on the beach plate.

The air flow rate is compared in different cavity pressures:

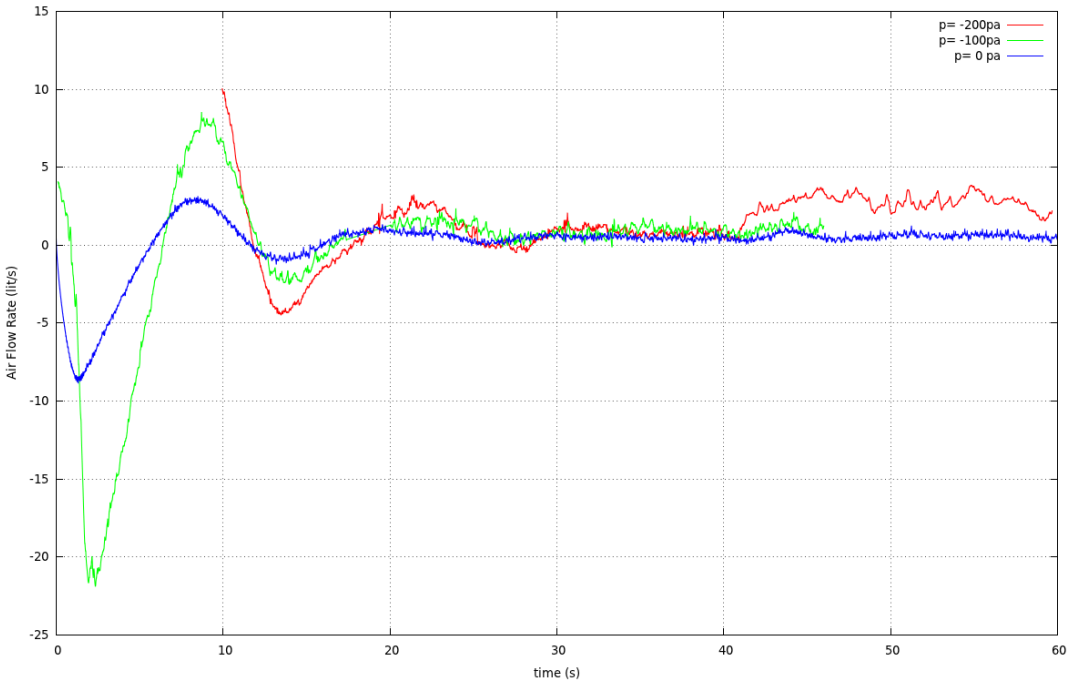

Figure 7 - 2D Simulation, Air flow rate into the cavity in different pressure.

The average values of air flow rate for the last 10 seconds of each run are:

Table 5 - Average air flow rate into the cavity in different pressure.

pressure	-200	-100	0
Air Flow Rate (lit/s)	2.72	1.03	0.59

The problem with the higher pressure is that in the experiment the condition is too sensitive to be sustained. In fact at initial stage of the run, the air flow rate is much bigger than the capacity of the valves and the cavity enters the periodical filling and losing the adjusted pressure mode.

The average forces acting on different parts for the last 10 seconds are given in the table below:

Table 6 - 2D Simulation; Forces on different parts of the air cavity in different cavity pressure.

Pressure	Aft Plate	Beach Plate	Fore Plate	Total	Flat plate
-200 pa	3.32 N	16.07 N	11.54 N	30.93 N	49.1 N
-100 pa	5.09	11.26	11.46	27.80	49.1
0 pa	5.55	6.88	11.36	23.8	49.1

1.3 Slope effect

Four different 2-D cases with similar boundary conditions were compared using different beach slope. The case description is given in the table below:

Table 7 - 2D Simulation cases with different beach slope.

Case	Water Velocity (m/s)	Cavity Pressure (pa)	Beach slope	Cavity height (mm)
ACS75	1.8	-200	18.4°	100
ACS103	1.8	-200	11.3°	100
ACS78	1.9	-200	18.4°	100
ACS105	1.9	-200	11.3°	100

The free surface height inside the cavity is compared in the graph below:

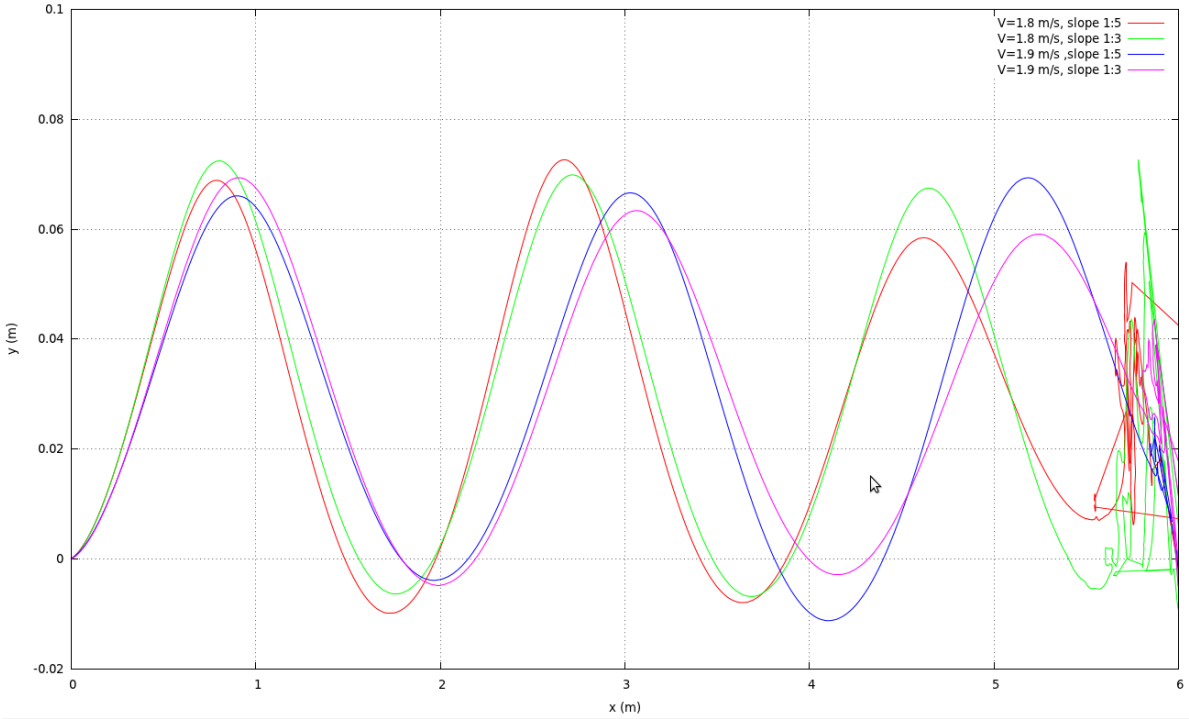

Figure 8- 2D Simulation free surface elevation in different beach angle and velocity.

The difference in the wave height might be from two sources: the effect of the beach blockage or the density of the mesh in different simulations.

The beach re-attachment comparison between these cases is presented as below:

Figure 9 - 2D Simulation; beach re-attachment angle in different velocity and beach slope.

As it is shown in the picture, a slight change in the velocity has more effect on the way that air bubbles are generated at the beach section, compared to the slope of the beach. This means that other parameters like the velocity and the angle of re-attachment are more important than the beach slope.

2 Recessed Cavity

The water flow into the cavity is similar to a transom stern flow after a ship. The sharp edge of the cavity in which the water separates from the hull creates a wave inside the cavity.

From the previous study we showed that to have the least pressure force on beach surface we should have as high pressure as possible inside cavity or low velocity. On the other hand even slight change in the speed results in sudden change in resistance force which is not desirable. To make the free surface shape of the wave inside the cavity independent of the velocity and pressure (in the operation range of ship), we consider an idea for the geometry of the fore-plate.

G.H. Schmidt in "*Linearized Stern Flow of a 2-D Shallow-Draft Ship*" (1981) suggested a family of profiles which doesn't leave a wave in the far-field wake behind the stern. The families of the dimensionless curves are shown in the picture below. Based on the ship draught and velocity, these curves can be converted to the real-size dimensions.

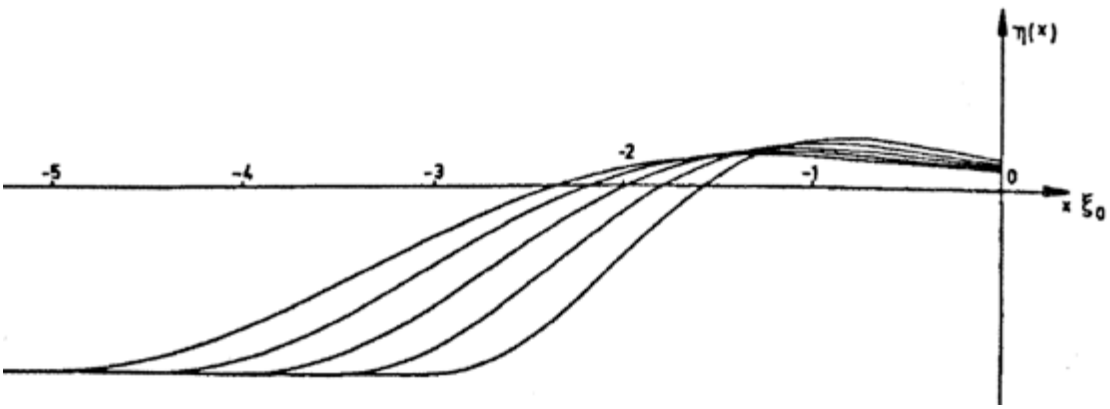

Figure 10 - Family of profiles.

Instead of increasing the pressure to decrease the wave amplitude in the cavity, we can use one of the recessed edge profiles fore of the cavity with the same effect.

The comparison between the sharp edge and recessed edge is performed in a series of 2-D simulations:

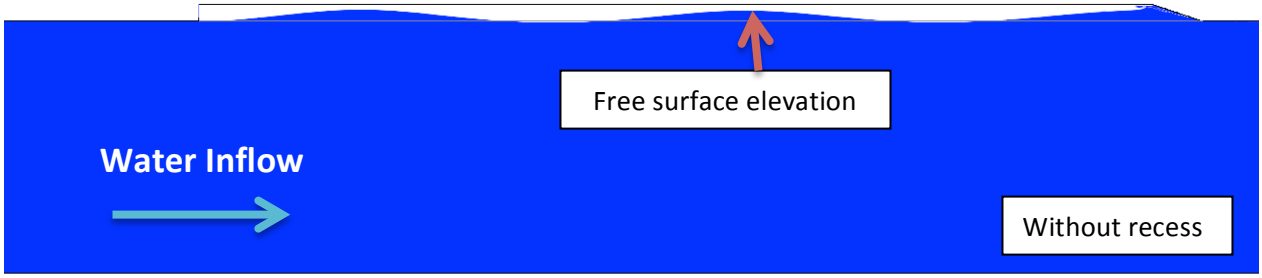

Figure 11 - 2D Simulation; Free surface elevation with sharp edge.

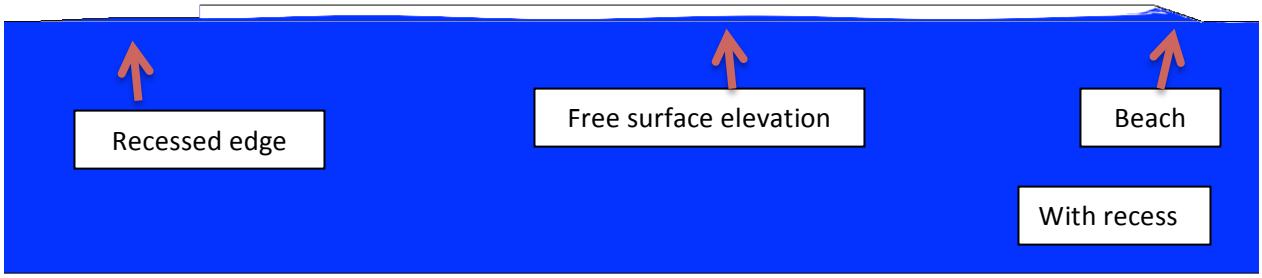

Figure 12 - 2D Simulation; Free surface elevation with recessed edge.

The hydrostatic pressure difference between the cavity pressure and the water pressure under the hull is the cause of the wave inside the cavity.

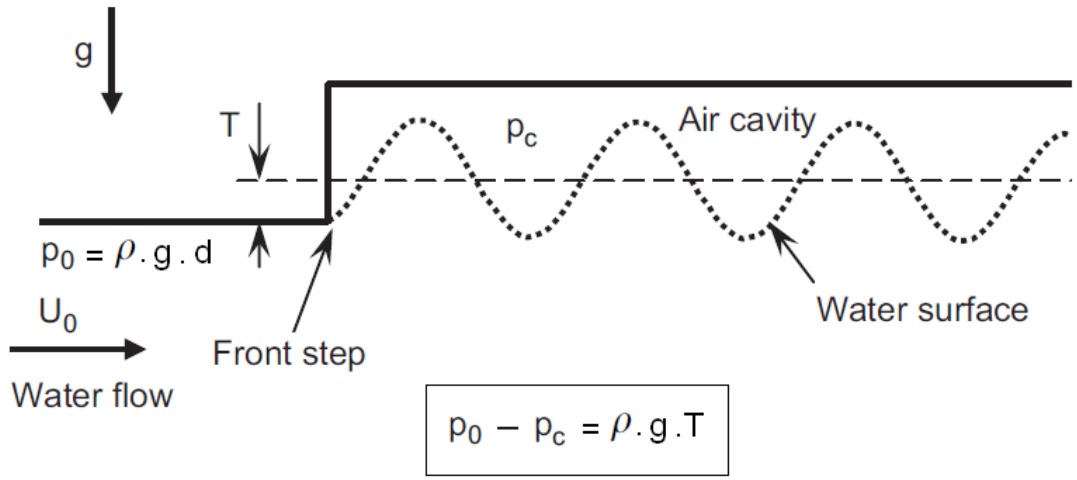

Figure 13 - Schematic of wave formation inside the cavity.

One method to decrease the amplitude of this wave is to increase the cavity pressure up to the P_0, as is investigated in §1.2. This is however not a stable situation for the cavity when

the ship moves, because of the difficulty in the air supply controlling system and sensitivity to surrounding pressure field.

Another method is then to maintain a minimum pressure difference in which the cavity remains stable, and try to decrease the wave amplitude by using the recessed edge.

In the design of the recessed edge, the hydrostatic pressure difference, “T”, is the parameter to find the proper curve from the series of above curves.

Six different 2-D cases with similar boundary conditions were compared using different velocities. The comparison is between cases with sharp edge and recessed edge. The case description is given in the table below:

Table 8 - 2D Simulation cases to compare the recessed edge effect.

Case	Water Velocity (m/s)	Cavity Pressure (pa)	Beach slope	Cavity height (mm)	Edge
ACS75	1.8	-200	18.4°	100	Sharp
ACS78	1.9	-200	18.4°	100	sharp
ACS71	1.96	-200	18.4°	100	sharp
ACS76	1.8	-200	18.4°	100	Recessed
ACS82	1.9	-200	18.4°	100	Recessed
ACS70	1.96	-200	18.4°	100	Recessed

The free surface height inside the cavity is compared in the graph below:

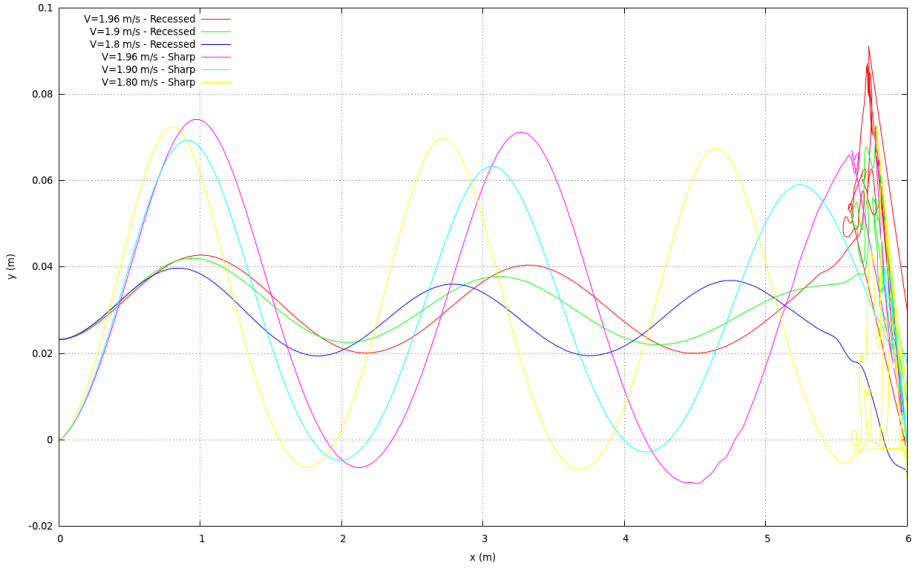

Figure 14- 2D Simulation free surface elevation comparison between sharp and recessed edge in different velocity.

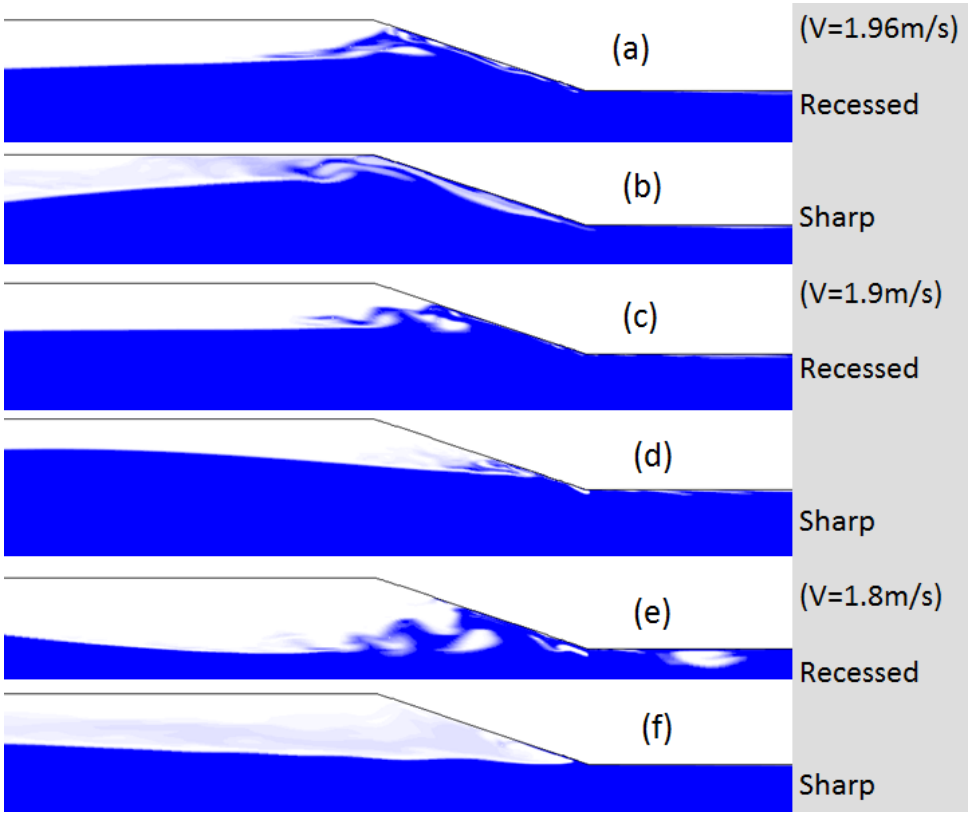

Figure 15 - 2D Simulation; beach re-attachment position comparison between sharp and recessed edge.

The air flow rate for different cases with and without recessed edge:

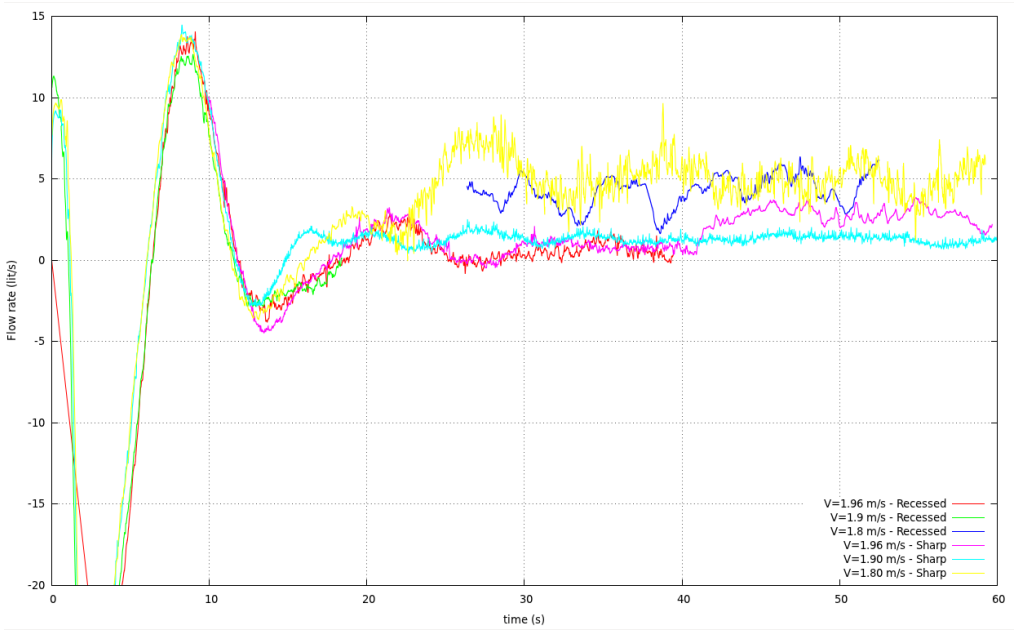

Figure 16 - 2D Simulation; Air flow rate into the cavity with and without recessed edge.

The average values of air flow rate for the last 10 seconds of each run are:

Table 9- The average of air flow rate with and without recessed edge.

Velocity	Recessed	Sharp edge
1.8 m/s	4.62 lit/s	4.97 lit/s
1.9 m/s	0.32 lit/s	1.24 lit/s
1.96 m/s	0.74 lit/s	2.72 lit/s

The average forces acting on different parts for the last 10 seconds are given in the table below:

Table 10 - - 2D Simulation; Forces on different parts of the air cavity with and without recessed edge.

Velocity	Aft plate	Beach plate	Fore plate	Total	Flat Plate	Ratio
1.96 m/s	3.32 N	16.07 N	11.54 N	30.93 N	49.1 N	0.63
1.96 m/s recessed	5.88	15.22	5.61 + 2.11	28.82	49.1	0.59
1.9 m/s	1.7	8.24	10.90	20.83	46.3	0.45
1.9 m/s recessed	6.94	13.88	5.29 + 1.86	27.96	46.3	0.60
1.8 m/s	1.28	5.02	9.85	16.15	41.9	0.39
1.8 m/s recessed	0.45	10.58	4.78 + 1.41	17.21	41.9	0.41

3 Resistance Reduction Tests

The previous series of tests on cavity resistance reduction was performed on a simplified version of a single cavity placed on top of a water tunnel. The result of the tests did not have any information on the behaviour of the cavity mounted in a ship hull. The difference is that the pressure distribution of the bow section might change the inflow condition.

In order to implement the air cavity concept in more realistic situation, a series of resistance measurement tests were performed in towing tank using a 1:44.167 scale suspended model.

The tests were performed in calm water and in head wave conditions. The tests are grouped in 6 series:

1. Base-line tests. Hull with pressurized cavity (sharp edge) in different velocity and calm water condition.
2. Wave Condition. Hull with pressurized cavity (sharp edge) in different velocity and different head wave conditions.
3. Recessed Fore-section. Hull with pressurized cavity (recessed edge) in different velocity and calm water condition.
4. Recessed Fore-section in wave. Hull with pressurized cavity (recessed edge) in different velocity and different head wave conditions.
5. Recessed Fore-section, extended cavity. Hull with longer cavity (recessed edge) in different velocity and calm water condition.
6. Recessed Fore-section, extended cavity in wave. Hull with longer cavity (recessed edge) in different velocity and different head wave conditions.

3.1 Series 1 – Base Line Tests

Test was performed with a suspended model towed in calm water to measure the resistance force. The resistance force includes both wave resistance and viscous resistance. Air cavity prevents direct contact of water with a section of hull that reduces the viscous resistance. Picture in below shows the bottom of hull with the air cavity. The wave created inside the cavity and its wavelength is proportional to the square of velocity. The result of force measurement is listed in table below; note that only the resistance reduction ratio is listed for protection of IP.

Table 11 - Model test cases ; baseline.

Series/ Run no.	Ship Speed [knots]	Model Speed [m/s]	Cavity Air Pressure [pa]	R / R_{intact}
1 / 1	11.5	0.89	2485	91.1 %
1 / 2	12	0.929	2482	92.9 %
1 / 3	12.5	0.968	2484	90.4 %
1 / 4	13	1.006	2484	90.2 %
1 / 5	13.5	1.045	2484	91.7 %
1 / 6	14	1.084	2484	89.8 %
1 / 7	14.5	1.122	2457	89.1 %

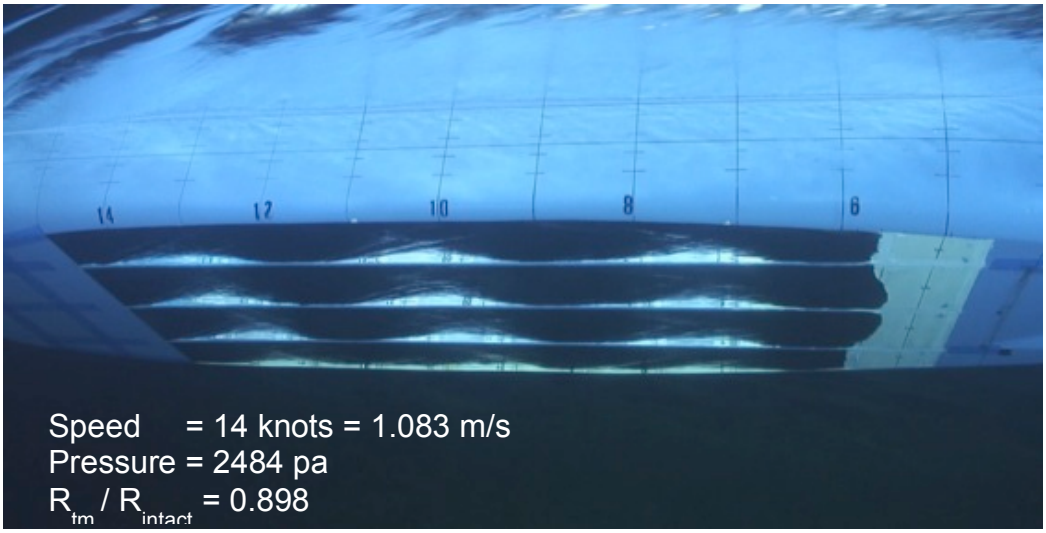

Figure 17- Under water picture of cavity free surface.

With the baseline design of the hull shape, the resistance reduction is between 7% and 11%, depending on the speed. In all these cases the air release is minimum, and observation shows the air does not escape from cavity and free surface wave inside the air cavity is stable. Wavelength depends on the speed and the position of re-attachment is also determined by speed. Air pressure inside the cavity is determined by the draft of the hull.

3.2 Series 2 - Wave Condition

Test was performed with a suspended model towed in head wave. In regular waves, three speeds (11.5, 12 and 14.5 knots) were tested in different wave heights (1, 2 and 3m) and wave periods (5.32, 5.98, 7.04, 8.64, 10.63 and 15.95s). Also the model was tested in irregular head wave with one speed in sea-state 3 for North Atlantic.

The model was suspended to avoid any motion. This series of test was to observe the behaviour of cavity in wave condition. The cavity could withstand all the selected periods of incoming wave in the wave height equivalent to 1m-wave in full scale.

Air started to escape in higher wave amplitudes when the wave period was exceeding 7 or 8 second. The worst condition was when the wave period was in the range of model wavelength (length / velocity).

In irregular waves the cavity could withstand the incoming pressure changes but there was some air release from cavity, which was replaced by the air pump immediately.

3.3 Series 3 - Recessed Fore Plate

Test was performed with a suspended model towed in calm water. The fore-section of the cavity accommodates a small recessed surface as shown in the picture below. The effect of the recess is to lower the amplitude of the wave inside the cavity in the same air pressure. As discussed in computer simulation result, the wave amplitude depends on the cavity's air pressure and it is desirable to be as small as possible. With the recess we can use lower pressure but still have small wave amplitude. The observation showed the position of re-attachment is independent of the velocity in the design with recess. The resistance is decreased in some speeds compare to the base-line design but there are some speeds which the resistance reduction is not improved as it is shown in table below; note that only the resistance reduction ratio is listed for protection of IP.

Table 12 - Model test cases ; Recessed Fore-Plate.

Series/ Run no.	Ship Speed [knots]	Model Speed [m/s]	Cavity Air Pressure [pa]	R / R_{intact}
3 / 1	11.5	0.89	2490	86.0 %
3 / 2	12	0.929	2484	90.1 %
3 / 3	12.5	0.968	2487	92.3 %
3 / 4	13	1.006	2487	85.5 %
3 / 5	13.5	1.045	2485	88.7 %
3 / 6	14	1.084	2486	90.5 %
3 / 7	14.5	1.122	2485	93.7 %

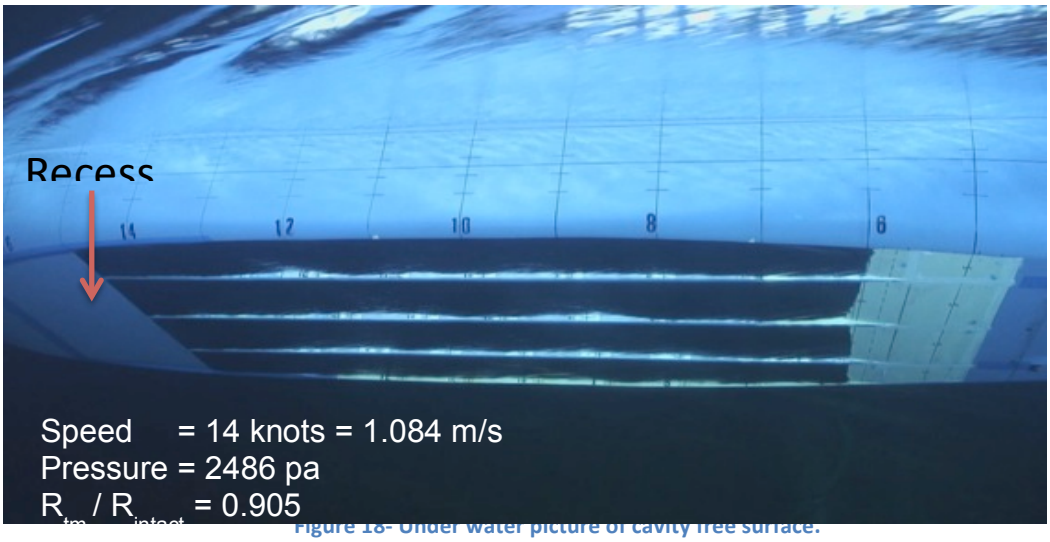

Figure 18- Under water picture of cavity free surface.

3.4 Series 4 and series 6 - Recessed Fore-section in wave

The same behaviour was observed as in the series 2 of tests. The recess effect was minute and the detail of the cavity response to the incoming wave was complicated. More experiment is required to conclusively explain the effect of design change in the stability and performance of the cavity in the wave.

3.5 Series 5 - Recessed Fore-section, extended cavity

The cavity was extended one station toward aft section but the rest of the cavity parameters are kept constant.

Table 13 - Model test cases ; Extended cavity with recessed edge.

Series/ Run no.	Ship Speed [knots]	Model Speed [m/s]	Cavity Air Pressure [pa]	R / R_{intact}
5/ 1	11.5	0.89	2474	88.1 %
5 / 2	12	0.929	2479	90.2 %
5 / 3	12.5	0.968	2484	89.4 %
5 / 4	13	1.006	2485	87.8 %
5 / 5	13.5	1.045	2482	85.7 %
5 / 6	14	1.084	2478	86.3 %
5 / 7	14.5	1.122	2472	86.8 %

Air release was higher in this configuration of cavity but the resistance reduction was improved in all speeds. This is expected since the wetted surface area is decreased in this

design. Also the wave amplitude inside the cavity is minimum in the same cavity pressure compare to the previous tests as shown in the picture below.

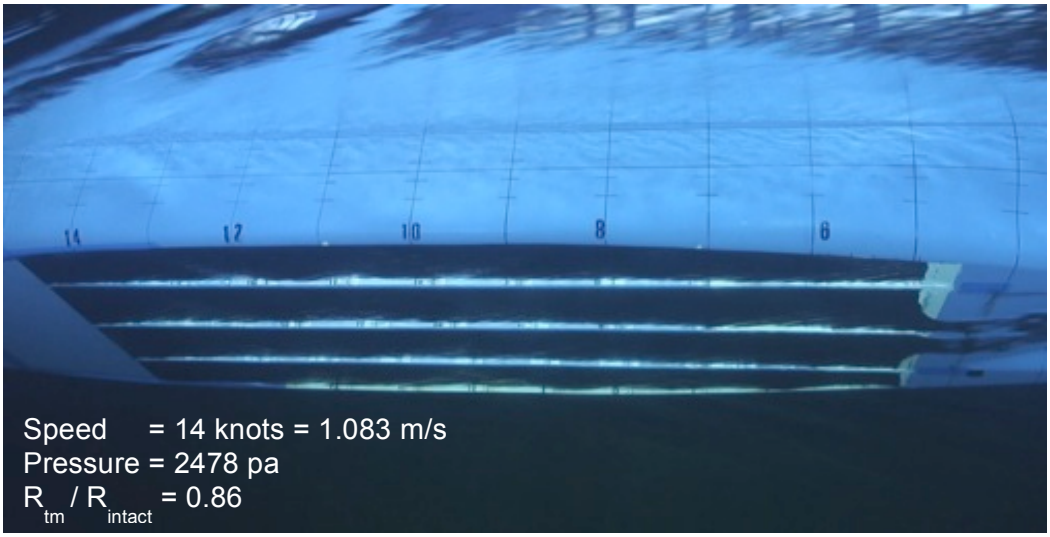

Figure 19 - Under water picture of cavity free surface.

The graph below compares the resistance of the model in series 1, 3 and 5 normalized with the resistance of the model without cavity. The values show a resistance reduction because of the cavity in all cases and velocity between 6% and 14.5%.

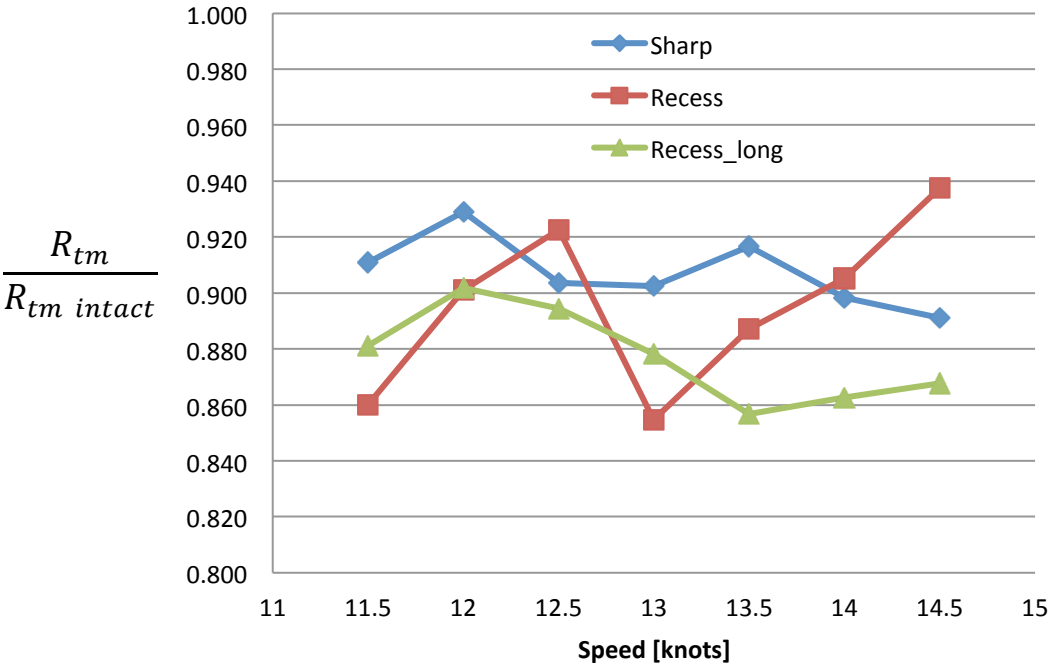

Figure 20 - Normalized resistance reduction in the experimental cases.

4 Effect of Hull Form on Cavity Performance

To take the effect of hull form and bow section shape into the account two different hull forms have been simulated using CFD. For the comparison the bare hull cases (without cavity) of the same configurations are also computed. These two hull forms have been used by SSPA in a series of model tests in the towing tank, therefore we were able to validate the result with the experiment. Both model hulls were modified versions of Stena P-MAX ships with the design parameters listed in Table 14.

Table 14 - Principal Dimensions of the Stena P-MAX

Design Parameters	Ship
Draft [m]	11.30
Length Between Perpendiculars [m]	175.5
Breadth [m]	40
Displacement [m^3]	65075
Wetted Surface [m^2]	10061

The structured meshes were generated for model size hull (3.97m) and placed in a rectangular domain of the size 15m X 5m X 5.256m. To reduce the simulation cost, only half of the flow field is simulated assuming symmetric boundary condition in the middle. Figure 21 shows the simulation domain.

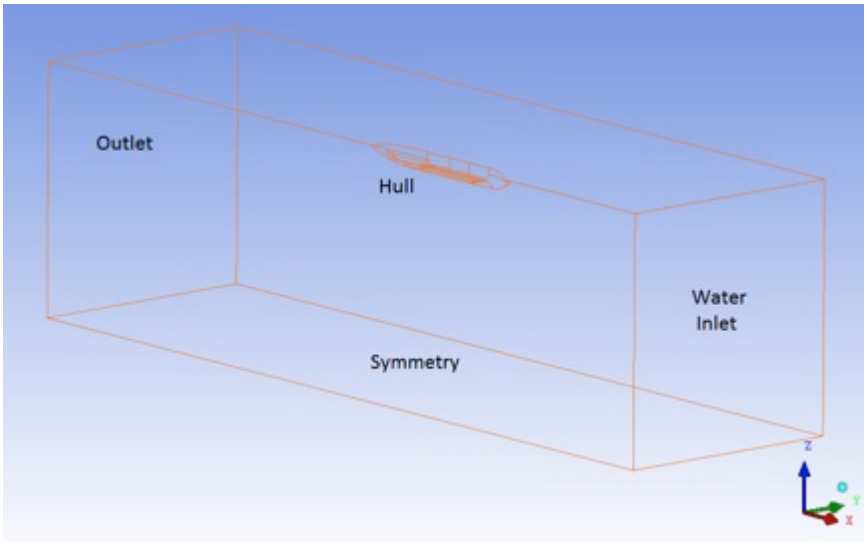

Figure 21- CFD Simulation Domain

The air is allowed to the cavity through the “Air Inlets” and the constant pressure condition is considered for this entrance. The simulation is using the assumption of double hull simulation which ignores the free surface around the hull. Figure 22 defines each section of the simulated hull.

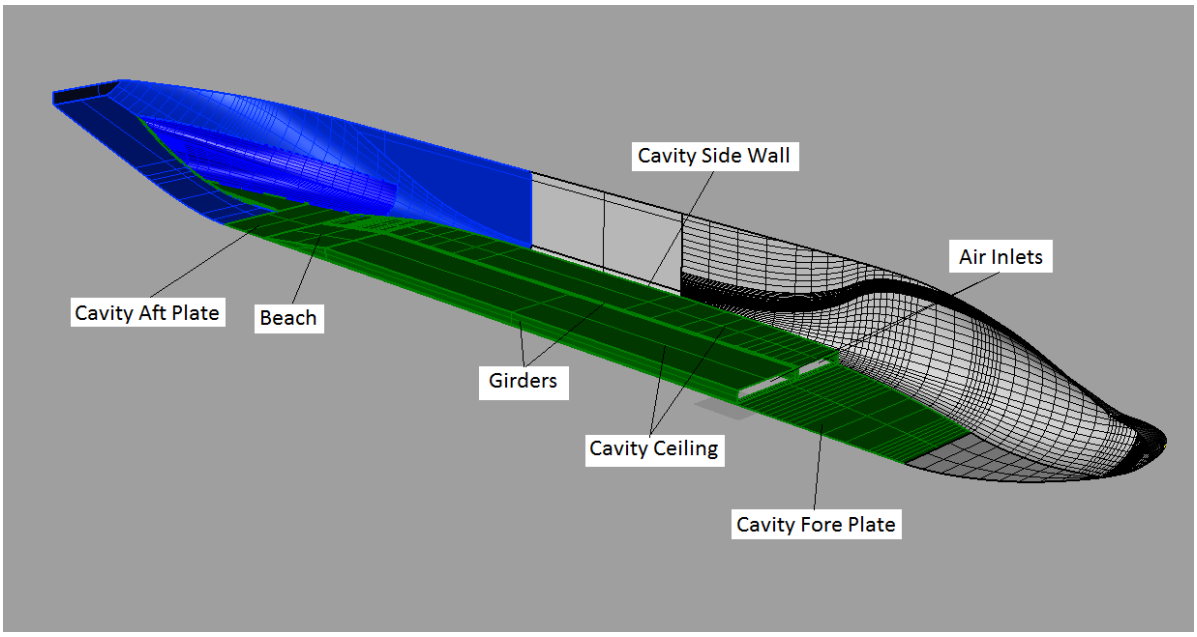

Figure 22 - Schematic of simulated model hull.

Unsteady simulations are performed for the hulls with cavity and steady-state simulation is done for the bare hull computations. The inlet velocity is constant and uniform (13 knots, full scale).

Figure 23 shows the pressure coefficient distribution in two bare hull forms (without air cavity).

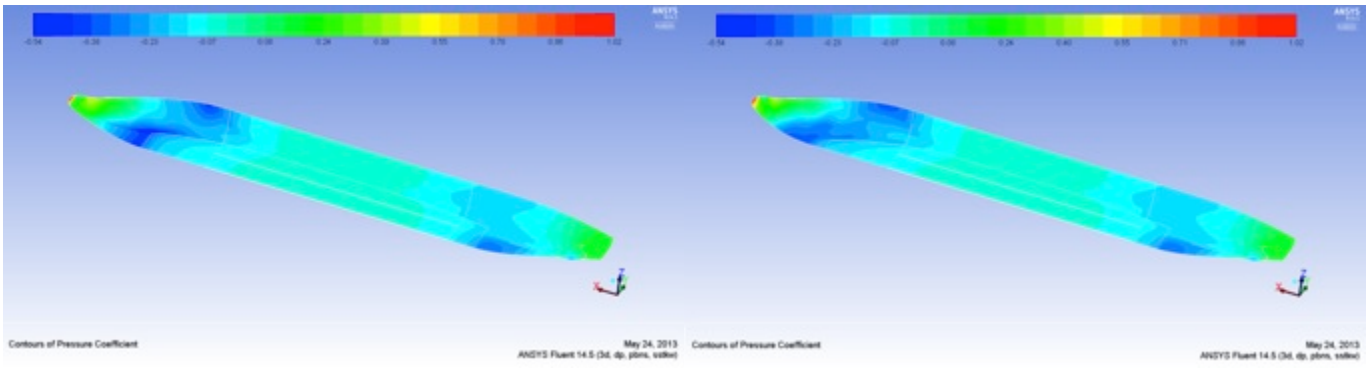

Figure 23 – Pressure coefficient distribution on bare hulls.

The result of these simulations, show less than 1% difference between the total resistance forces. Also the total resistance value for both hulls are calculated to be approximately 10% less than the measured values in towing tank tests. This is due to the assumption made in the simulation that the free surface is not calculated; therefore the wave making resistance is not included in the simulation.

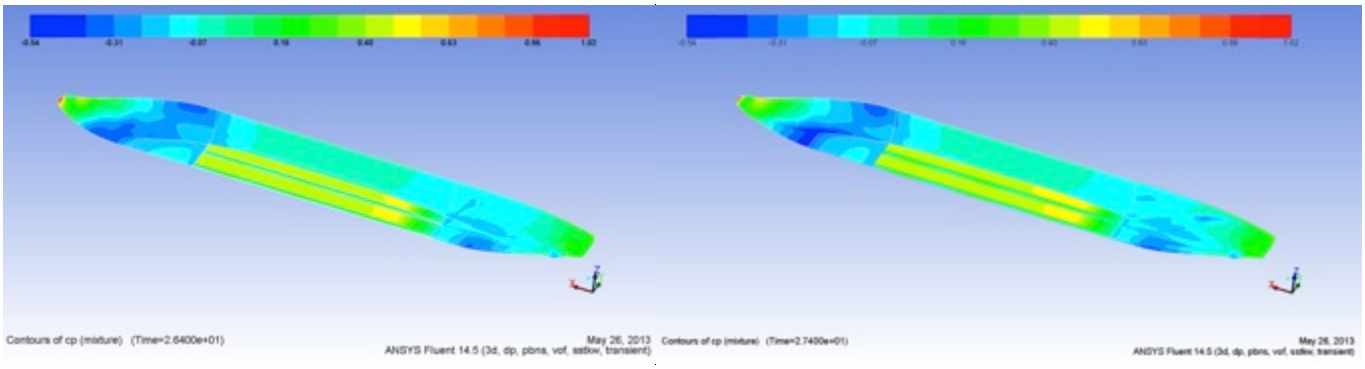

Figure 24 - Pressure coefficient distribution on hulls with cavity.

Figure 24 shows the pressure coefficient distribution on the two hulls with air cavity.

The result of the simulations with air cavity shows 29% difference between the total resistance forces of these two hull forms, while the experimental results give a difference around 16.6%. A large contributor to this discrepancy is that the simulations overall under predict the forces, mainly since the free surface is not included in the computational model, thus the relative difference, as presented above, increases. Even though the percentage of the differences is high, the actual values have small differences since the total force acting on a small model is only few Newton.

The simulation provides a method to compare the hull form performances and even though the actual values are not close to the experimental results, the prediction of the performance has the same trend in both experiment and computation.

Bilaga 2

Artikel presenterad vid 29th Symposium on Naval hydrodynamics,
Göteborg, augusti 2012

29th Symposium on Naval Hydrodynamics
Gothenburg, Sweden, 26-31 August 2012

Hydrodynamics of a Displacement Air Cavity Ship

Abolfazl Shiri[1], Michael Leer-Andersen[2], Rickard E. Bensow[1] and Jacob Norrby[3]
([1]Chalmers University of Technology, [2]SSPA AB, [3]Stena Rederi AB, Sweden)

ABSTRACT

To study the resistance reduction of an air cavity for a displacement vessel, a simplified model of a single cavity is tested in a cavitation tunnel. The drag force acting on the cavity and the aft plate were measured and the water-air interface was monitored in different conditions. Behavioural changes to the free surface were observed by changing the geometry and flow characteristics like air pressure, air flow rate and water flow speed. Computational model for different cases with the same geometry and conditions were simulated using computational fluid dynamics(CFD).

The length of the cavity was designed to include approximately 2.5 times the expected wavelength of the water-air interface with Froude number based on the ship length of 0.19 which approximately represents a displacement ship with multi-wave air cavity at its cruising speed.

Parameters like cavity pressure play an important role for the wave's shape and the stability of the free surface inside the cavity. Both computation and experiment show that the amplitude of the wave is sensitive to the air pressure in the cavity and the re-attachment of the water to the rear end of the cavity has a close correlation to the inlet air pressure and water velocity. The ultimate goal of this investigation is to minimize effective power including air supply while reducing resistance in/around the cavity, but equally important is it to gain a more basic understanding of the air-cavity's behaviour and possible additional resistance components.

NOMENCLATURE

C_f	Friction coefficient resistance
En	Euler number based on the cavity pressure
Fn	Froude number based on the characteristic length
g	Gravitational acceleration
H	Cavity height
L	Cavity length
P_o	Hydrostatic pressure in reference point
P_c	Air pressure inside cavity
Re	Reynolds number based on the length
T	Cavity static submersion
U	Water velocity

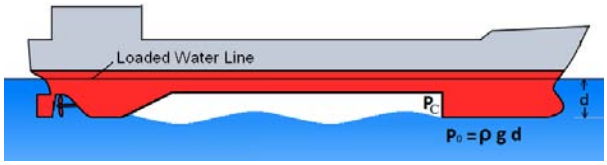

Figure 1: Schematic of a displacement multi-wave air cavity ship. P_c is the air pressure inside cavity and P_0, *reference pressure*, is the hydrostatic pressure under the hull.

W	Cavity width
λ	Wavelength of air-water interface
δ	Wall boundary layer thickness
ρ_w	Water density

INTRODUCTION

The frictional resistance of marine vehicles can be reduced by decreasing the area of wetted surface. For low Froude number displacement vessels the flat of bottom (FOB) area under the hull is relatively large and are as such well suited for air lubrication. Since it is not a viable option to decrease displacement, only very little can be achieved toward that goal by purely geometrical design, as other resistance components must be considered.

Different methods of air lubrication have been already implemented on air supported vehicles (ASV) for the purpose of drag reduction. From the Air Cushion Vehicles like hovercraft to planning boats with air cavity hull are using this technology to achieve higher speed. Other concepts including continuously injecting air under the hull, either as micro-bubbles or creating an air film, or replacing a section in the bottom of the vessel with a cavity filled with air are the focus of recent studies. Matveev [2003] discusses the range of the marine vehicles employing these concepts to decrease the viscous drag force or reach higher speeds. Another potential advantages of multi-wave air cavity is that by sudden release of the air (through a suitable emergency valve), the increased drag force provides a substantial braking effect on the vessel which can be used in the case of

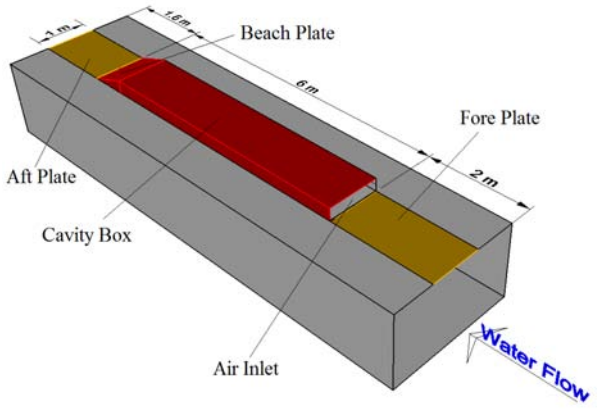

Figure 2: Schematic of the cavitation tunnel test section with the cavity on the roof. Three sections of the experimental rig, *fore plate*, *cavity box* and *aft plate* are colored separately.

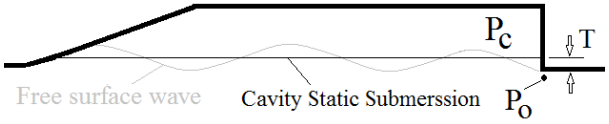

Figure 3: The cavity static submersion and the multi-wave schematic.

Figure 4: STENA AIRMAX demonstrator.

emergency.

There have been some studies with different arrangements of the cavity for planing or semi-displacement hulls. Matveev et al. [2009] studied the characteristics of a simple stepped planing hull model in a towing tank with different lengths and trims. Their investigation confirmed the theoretical limiting characteristic length defined for the cavities which form under the stepped plate. An inviscid two-dimensional CFD model was verified by experimental studies of the stable and oscillating partial cavity, performed by Lay et al. [2010]. The results showed high drag reduction, while considerable air flux was needed to establish a stable cavity.

Matveev [2003] gives a description for different air cavity wave types behind a wedge. He argues that the pressure difference between air inside cavity with incident hydrostatic pressure defines the free-surface wave shape. Another study by Foeth [2010] suggests the importance of the bow shape as a parameters for maintaining the air cavity. Thill et al. [2010] claims that the air cavity ships are highly speed dependent due to the variation in the wavelength of the free surface disturbance. İnsel et al. [2009] compare the experimental results of the air lubrication effect when the air is released through holes or porous media under the hull. The air flow rate scaling for a single backward-facing step air cavity hull is presented by Jang et al. [2010] with geo-similar models. They suggested a critical air flow rate in which any increase in flow rate does not provide further resistance reduction in such cavity design.

Previous investigations of air film lubrication at SSPA by Leer-Andersen and Larsson [2003] have indicated that a large number of transverse air outlets longitudinally are required, effectively rendering the air film/micro-bubble approach impractical for large displacement ships. The alternative method of using one or more pressurized cavities under the hull may provide a better solution. The shape and size of the hull also indicates the type of cavity that can be used for viscous drag reduction.

The above studies on single step air cavity hull suggest a characteristic length for partial cavity arrangement that limits the use of a stable cavity under a large displacement ship. For this kind of hulls the option of a full cavity that sustains the air volume with a longer distance under the hull is proposed. The depth of the cavity allows the free surface to form several wavelengths before it re-attaches to the inclined rear section of the cavity. Therefore the length of the full cavity is not theoretically limited, so long as the wave remains stable and the cavity does not collapse. There is a lack of physical understanding of the water-air interface behaviour in a full-cavity arrangement and in the parameters involved for the stability of the cavity and it's resistance reduction. The main goal of this study is to observe the behaviour of a simple cavity in order to extrapolate the results for a more general configuration.

Figure 1 shows the schematic of a displacement ship with a pressurized air cavity longer than the nominal wave-length of the free surface wave inside the cavity. In this schematic, P_c is the air pressure inside the cavity and is balanced with the reference pressure, P_o, the hydrostatic pressure of the water adjacent to the bottom of the hull and the wave height formed inside the cavity.

Various studies have been carried out at SSPA on the hull shape and cavity geometry for the STENA AIR-

Figure 5: Cavity box installed in the upper chamber of test section.

Figure 6: Beach plate and the side wall lines for measuring water surface height.

MAX project, including extensive model tests in the towing tank and performing series of measurements on a demonstrator of size 1:12 (see Figure 4). Although the results of these studies could provide a basis for full-scale hull design, a more detailed investigation was necessary to exploit the physics of the free surface behaviour and the parameters involved for the stability of the cavity. The focus of this study is to better understand these parameters through computational and experimental investigations. To simplify the problem, an experimental investigation was conducted in SSPA's cavitation tunnel to study a single cavity. The result of the experiment complements the numerical studies of the same geometry and operating conditions. The schematic of the test section, which is also used as computational domain, is shown in Figure 2. The practical issues of implementing air cavity system under the hull, like the method of air supply, the controller response time and cavity placement introduce other limitations in the design which is not the concern of this study.

AIR CAVITY PRINCIPLE

Two important parameters to characterize the flow in the cavity are the Froude number based on the length (cf. Larsson and Raven [2010]):

$$Fn = \frac{U}{\sqrt{gL}} \tag{1}$$

and Euler number based on the cavity pressure difference:

$$En = \frac{p_o - p_c}{\rho_w U^2} \tag{2}$$

where L is the characteristic length, U is flow speed, p_c is air pressure at the cavity inlet and p_o is the reference pressure. The transverse waves generated inside the cavity are assumed to have a wave length of $\lambda = 2\pi U^2/g$. The characteristic length can be considered as the ship length to include the whole wave resistance component of the vessel or the cavity length to study the free surface disturbance inside a single cavity without the effect of hull. Matveev [2007] also suggests the Froude number Fn_T based on the static depth of water inside cavity, T, to include the cavity pressure as a scaling parameter: $Fn_T^2 = En^{-1}$.

The process in which an air cavity is filled with air and is ready to operate can be defined as below: when the cavity under the hull is filled with air at the stationary position, the static pressure of water and air on both side of the air-water interface is balanced, i.e. $P_o = P_c$. If the interface is not at the same height of the cavity front step, the depth of water inside cavity will be called *cavity static submersion*, T (cf. Matveev [2007]). In this case the hydrostatic pressure balance can be written as: $P_o = P_c + \rho_w g T$. The static pressure at the front step is always equal to the draft hydrostatic pressure: $P_o = \rho_w\, g\, d$; where d is the hull draft (see figure 3). This study ignores the compressibility effect of air under the hydrostatic pressure of a full size ship. The depth of T is adjusted entirely by cavity air pressure in the model tests in the towing tank or the full-scale ship, but in a closed system like the cavitation tunnel, any amount of the water which comes out of the cavity and is replaced with air, should be compensated, to get a constant reference pressure of P_o. Failing to do so results in an unknown pressure field in the system and makes it difficult to adjust the running experiment based on the inlet air pressure. In computational domain also the hydrostatic pressure distribution at the water outlet boundary is defined to have a reference pressure.

The described problem might also play an impor-

Figure 7: Air inlet section and the position of upstream camera.

Figure 8: Side windows of the test section. The second camera was recording movies of the beach plate through these windows.

tant role in the events of an unstable cavity due to variation of reference pressure, like in an incoming wave. The local change in the hull draft introduces the variable reference pressure along the cavity. In CFD simulation as well as cavitation tunnel experiment, the entire system remembers the initial condition, since it dictates the reference pressure while the calculation is running. This might explain the sensitivity of the CFD calculation to the initial condition.

In the simulation of single cavity placed on the ceiling of the water tunnel, the constant reference pressure is considered as a part of running condition. Because there is a fixed flow speed and the air inlet pressure is determined, the only place to implement this constant hydrostatic pressure (representative of ship draft) is the outlet. In the experimental facility the cavitation tunnel is pressurized to provide the proper pressure difference for each test.

Both experiment and simulation in this study focuses on the conditions for a stable model size cavity. The assumption to sustain the Froude number scaling is the base for designing the test. Since the geometry of the single cavity is simplified in this study, for a proper extrapolation of the results (especially the drag reduction) to the full-size cavity under a hull, more towing tank model studies are necessary.

EXPERIMENTAL SETUP

Measurements and observations were completed on the behaviour of the air-water interface in a single cavity carried out in the SSPA cavitation tunnel to simulate the working condition of the air cavity under the hull. The design of the single cavity was based on the parameters used in STENA AIRMAX towing tank tests. The goal was to eliminate the complexity in the towing tank tests and have a controllable environment for a better understanding of the processes.

The largest test section available with the size of $9.6 \times 2.6 \times 1.6$m ($L\ W\ H$) was used in this experiment. The reason for using the largest test section is that the impeller driving the flow in the cavitation tunnel requires a minimum rate of revolution for lubrication of its bearings. To reach the desired low flow speed it was necessary to use the largest section. On the roof of the test section a recessed enclosure accommodates the cavity and other parts of the test rig. Inside the enclosure a steel frame was fitted to support the measurement equipment and cavity parts. The model test box consists of different sections: fore plate, cavity box, beach plate and aft plate, which are connected to the force gauges in order to measure the drag force on different surfaces (see Figure 2). Both cavity box and aft plate were suspended from the steel frame inside the enclosure and with free movement in the stream-wise direction, limited by strain gauges, to measure the forces. The cavity box is a one piece fibreglass container, reinforced by steel frame and the lower side of it is open. The steel frame prevent the cavity to bend and distort while exposed to the air and water forces. Figure 5 shows the cavity box (blue rectangular structure) installed inside the test enclosure on top of the test section.

The size of the cavity box is $6 \times 1 \times 0.25$m ($L\ W\ H$) which allows it to be sufficiently far from the side walls to ignore effects from the side of the tunnel. The boundary layer thickness on the bottom and side surfaces is estimated as $\delta = (0.37)\ L\ Re^{-0.2} \approx 12$cm at the end of the test section and the side walls are $80cm$ away from the box. The height of the cavity box is adjustable and two heights of H=0.25m and H=0.1m were tested. This is done by attaching or removing a plate inside the cavity box.

This study is focused on the air cavity designed for

the STENA AIRMAX and the flow speed was scaled based on similar Froude number of the hull. Therefore the flow speed of 2m/s corresponds to 16 knots cruising speed of the real size ship. The flow speed was measured with Pitot tube placed upstream of the test section. The boundary layer velocity variation across the tunnel is considered as measurement uncertainty. Since the boundary layer development and pressure distribution on the hull depend on the detail of the design, the difference between these parameters on the test section wall before the cavity box and on the bow in real size ship is not considered in this study.

The cavity length is selected based on the maximum allowed size in the test section, such that more than one free-surface wavelength is presented in the cavity (in fact around 2.5 to simulate a multi-wave cavity). The scaled velocity provided the Froude number of Fn = 0.19 equal to the full size ship. Matveev [2007] studied three-dimensional mathematical wave pattern in the rectangular air cavities with different ratio of width to wavelength. The wave pattern was also sensitive to the step shape. The ratio of $W/\lambda = 0.4$ has been used for the initial design of the cavity, although λ varies when tests are performed with different flow speed.

An inclined wall at the rear section of the cavity, hereafter known as beach plate, allows the water to reattach to the cavity wall with minimum disturbances. Figure 6 shows the beach plate installed at the rear of the cavity box. The angle of the beach wall is adjustable together with the depth of the cavity. Three slopes were used in this study; 1:3 (equal to 18.4°), 1:5 (equal to 11.3°), and 1:7 (equal to 8.1°).

There is a difference in terms of draft between a model hull with a cavity underneath floating on the water and a single cavity placed on top of the test section and connected to the force gauges. The draft of the hull can be simulated by running the entire cavitation tunnel under pressure. This pressure is the reference pressure which the air inlet pressure is adjusted with. The gap between the cavity box and the fore and aft plate is approximately 3mm which allows free movement of the cavity in order to measure the forces on each part. Water enters into the test enclosure through the gap since the tunnel is pressurized for which reason the cavity box and measurement equipments are submerged. Observation of the flow on top of the cavity box showed no circulation or movement inside the upper enclosure which could cause additional force on cavity.

The air is supplied by the compressed air system and the air flow is controlled by an automatic valve. The controller system is designed to apply constant flow-rate or constant cavity pressure. To achieve constant pressure, air is allowed to both enter and exit from the cavity through the valve. A flow meter measures the air flow

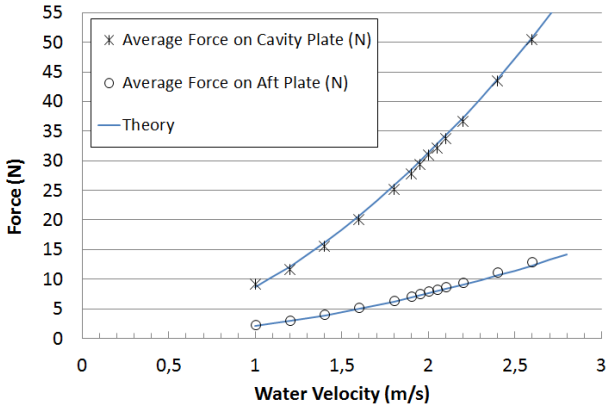

Figure 9: Average measured viscous forces on the flat plate representing the intact hull sections replaced in the position of cavity box. The theoretical curves are based on the equation 3.

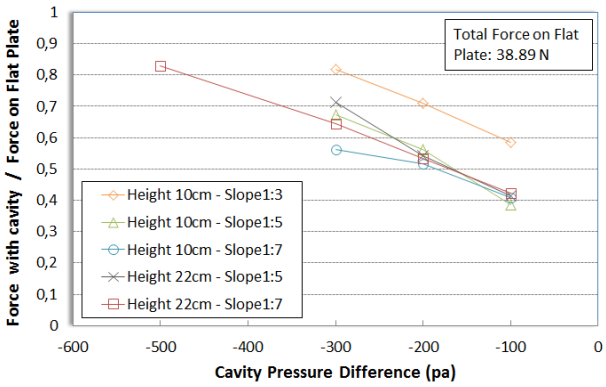

Figure 10: Average measured forces on both cavity box and aft plate in different cases. The force is normalized by the total force on intact hull section.

in both ways. The cavity pressure is measured from a pressure tap positioned immediately after the air inlet on the cavity ceiling. The inlet chamber is curved to avoid perpendicular injection of air on the water surface to eliminate impinging jet disturbances. Figure 7 shows this curved section and the 2cm step in front of the cavity box. The inlet chamber also provides a uniform air flow into the cavity box.

In order to have an estimation of free-surface wave shape, horizontal and vertical lines were drawn on the walls and ceiling of the cavity box (see Figure 6). Photos of these lines were taken through windows of the test-section which are shown in Figure 8.

Two cameras were recording film during each run. First camera was installed inside the cavity (see Figure 7), in the air inlet section looking toward beach plate. The evolution of the free-surface is observed by this camera.

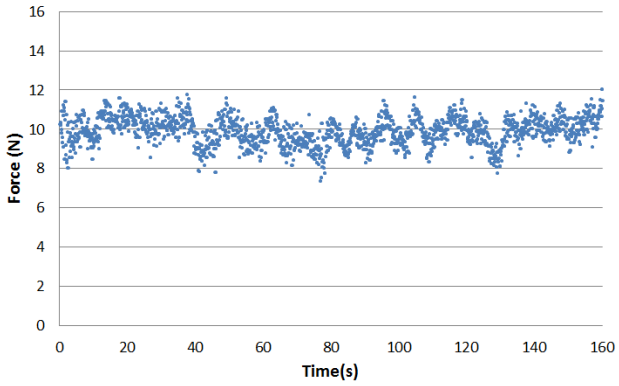

Figure 11: Instantaneous force measurement of the cavity box. The pressure difference is -200pa, cavity heigth is 10cm and the slope is 1:7.

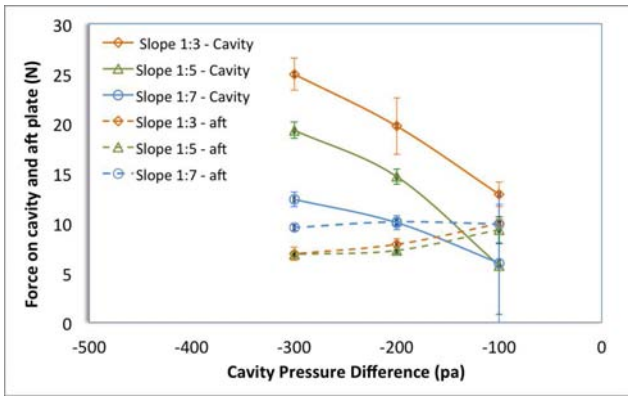

Figure 12: Forces on cavity box and aft plate for the cavity height of 10cm in different pressure and beach slope. Average values and standard deviation is presented in the figure.

The other camera focused on the beach plate through the test section's window (Figure 8). This camera provides visual information of the re-attachment process of water on the beach plate and the air leakage from the cavity is visible in the recording.

Uncertainties in Measurement

Before we present the result of the measurement it is necessary to provide the estimation of the uncertainties from the measurement equipment and the experimental methods used in this study. For the force measurement on cavity box and aft plate, the gauges were calibrated using weights before the tunnel filled with water. The estimation of drag calibration uncertainty on cavity box was $\pm 2N$ and on aft plate was $\pm 0.1N$. The difference is due to the size and mounting system of the cavity box.

The measured forces on the cavity box fluctuated caused by pressure force on the beach plate, as it is shown in Figure 11. The standard deviation of the fluctuating force is presented in the result along with average value (see Figure 12; These values do not inclued calibration uncertanity). The air flow measurement error estimation is $\pm 3\%$ of measured value. The air valve in the experiment allowed a maximum flow rate of about 3.5 lit/s to enter the cavity.

To measure the free surface position along the side walls, the scale with the size of 1 cm in height and 10 cm in stream-wise were drawn. The observation of the free surface was more difficult in lower cavity pressures due to ragged and bubbly surface.

Experimental Results

To provide a baseline for comparison, the surface friction resistance coefficient is estimated as (cf. Schlichting [1979])

$$C_f = \frac{0.455}{(\log Re)^{2.58}} - \frac{1700}{Re} \tag{3}$$

which gives the surface friction resistance force for an intact test section as $R = (1/2)\, C_f\, \rho_w\, U^2\, L\, W$.

The surface roughness on different parts of the cavity and aft plate were measured. The average roughness on the cavity plate was 5.99μm and on the aft plate was 2.75μm. According to Schlichting [1979], a surface with this roughness can be considered as hydraulically smooth surface in the range of the experiment's Reynolds number. Using these values, the result of the measured forces can be compared on flat plate measurement with the literature. We assume that the boundary layer starts to develop on the surface from the beginning of the test section. According to the Figure 2, the length of fore plate is 2m, the cavity plate is 6m and the aft plate is 1.6m. By estimating the coefficient of local skin friction, we can calculate the forces acting in each plate separately. Forces estimated by this method is presented in Figure 10.

By installing a flat plate in the position of the cavity, a series of force measurement were carried out to have a baseline for the force measurement. The flat surface represents the intact area in which cavity was installed. The forces applied by the water in different velocities were measured for the cavity plate and the aft plate. Figure 9 shows the average forces at different flow speeds. The measured forces on both plates at different velocities are close to the estimated values based on the equation 3.

A total number of 68 runs in different conditions were performed in 8 series of measurements. Each series of measurement consist of a constant geometric setup and variable air cavity pressure or flow speed condition. The recorded data include force measurement on cavity-box and aft plate, air inlet flow-rate, reference

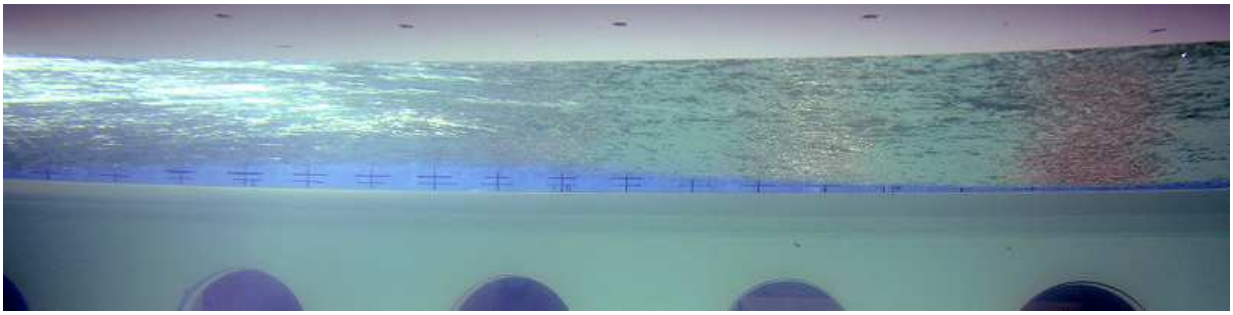

Figure 14: The cavity side wall picture. The water free surface shape can be estimated by reading the height of the wave on the wall.

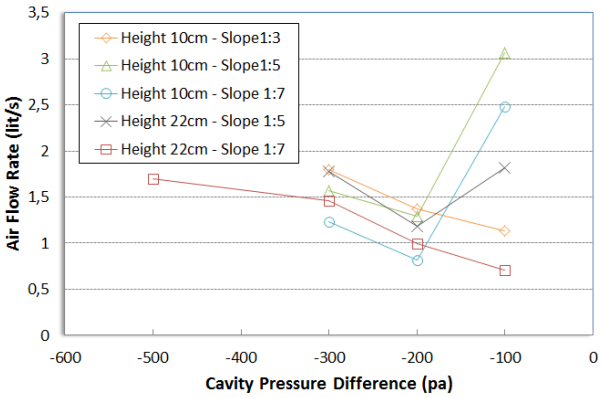

Figure 13: Average air flow rate supplied into the cavity for different cases.

pressure, flow speed and air pressure on 12 points of cavity ceiling. Table 1 summarises condition for each series of measurement.

The normalized drag force is shown in Figure 10 and the average air flow rate for different cases is presented in Figure 13. For the cases with a constant flow speed, the total force (including the force acting on the cavity box and the aft plate) increases when the cavity pressure decreases. In lower cavity pressure the amplitude of the free surface wave is larger and the area of the wetted surface on cavity side walls are bigger. In higher cavity pressures the re-attachment position moves to the lower section of the beach plate which decreases the water pressure force on beach. In such condition the air release also increases. The forces on aft plate does not show the same trend as the forces on the cavity box. Figure 12 shows the forces on cavity box and aft plate separately in different cavity pressure and different beach slope with the cavity depth of 10cm. The reason for decreasing the force on the aft plate in lower pressures is not clear but it can be related to the change in the boundary layer flow on the aft plate due to the re-attachment process. An increase in air release rate did not contribute directly in the air lubrication of the aft plate since the bubbles seem to be convected to the outside of boundary layer on the aft plate. The snap shots of the videos from beach plate show this process in Figure 17 for different cases. The air release rate is correlated to the air pressure and there is an optimum pressure for each case with the least air flow rate. For the high water velocity cases, no pressure or cavity configuration was found without air release, and the bubble rate seems to relates more to the position of re-attachment rather than directly controlled by air pressure or beach angle. Any change in cavity pressure, beach slope or flow speed results in the variation in the re-attachment position, hence the air release rate.

Figure 11 shows the instantaneous force measured on cavity box for the case with cavity depth of 10cm, the beach slope of 1:7 and the cavity pressure of -200pa. The forces on beach is higher for the case with the slope of 1:3 compare to the other two beach slopes. This difference is not considerable between two slopes of 1:5 and 1:7. The height of the cavity does not play important role in the cavity force, although in the cases with bigger cavity depth it is possible to sustain a stable cavity in lower pressures (-500pa) without allowing the water to come in contact with the cavity ceiling.

Air pressure inside the cavity was measured through 12 pressure taps positioned along the cavity center-line on the ceiling. The measurement of the air pressure variation inside the cavity turned out to be very difficult since the difference between the air pressures (< 3 *pa*) were less than the calibration accuracy. The measurement series 5 (see Table 1) showed a continuous increase in the total force on cavity box and aft plate when the flow speed was increased. In the measurement series 6, the experiment showed that sustaining a pressure balance in cavity is very difficult with providing a constant air flow rate due to unsteady behaviour of air release.

Table 1: The condition for series of experimental investigation.

series No.	cavity height	Beach slope	cavity condition
1	10 cm	1:3	3 different pressures
2	10 cm	1:7	3 different pressures
3	10 cm	1:5	3 different pressures
4	22 cm	1:7	4 different pressures
5	22 cm	1:7	different flow speed
6	22 cm	1:7	different air flow rate
7	22 cm	1:5	3 different pressures
8	–	–	flat plate drag

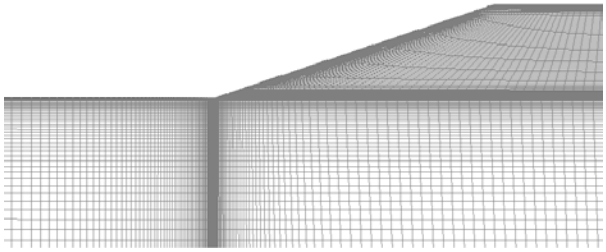

Figure 15: 2-D Structured mesh in beach plate region. Flow direction is from right to left.

COMPUTATIONAL STUDY

The computational study was carried out using a RANS method. Fluent was used with *Volume of Fluid* (VOF) method to simulate the unsteady free surface inside the cavity. The study was aimed at determining the best method for the CFD to simulate the experimental result. As such the experiments are mainly for verification and validation of the CFD model. At a later stage it is planned to use the acquired knowledge of the CFD simulation for optimisation of the real application. The computational model consists of the cavity box and the entire test section as it is shown in Figure 2. The gap between the cavity box and the test section introduces unnecessary details into the computational model therefore it is not included in the simulation. Since the computational domain is relatively large in size, a three-dimensional simulation for the test domain is quite CPU demanding. The experimental investigation also shows the unsteady nature of the re-attachment process on the beach plate, hence the simulation time requires an unsteady solver with a very short time step and very high resolution around the beach.

2-D SIMULATION

To determine a baseline for the computational study, a series of two-dimensional simulation were investigated to provide the proper setting for the three-dimensional simulations. The two-dimensional simulation neither represent the correct shape of the interface nor the forces and air flow rate since the real cavity is limited by side walls. These simulations provide the framework on the sensitivity of the solution to the computational parameters and schemes.

The 2-D domain uses the stream-wise cross section of the 3-D domain with the same geometry. Only one cavity configuration was studied with the beach slope of 1:3 and the cavity depth of 10 cm. The simulation was carried out for different air inlet pressure and different flow speed. A total number of 210,000 quadrilateral cells were used in a structured mesh and the density of the mesh close to the beach region is higher to capture the proper resolution for bubble making process. Using a coarse mesh shows a layer of mixture of air and water is released from the cavity instead of bubbles. More refinement of the mesh at beach region did not improve the result of the simulation. Figure 15 shows the computational grid at the rear side of the cavity and beach region.

The transient solver in Fluent was chosen to solve a multiphase flow with the water as primary phase and air as secondary phase. The multiphase model uses the *Volume of Fluid* (VOF) method to simulate the unsteady water-air interface inside the cavity. The VOF method defines a volume fraction of each phase in the cell as the indicator of the interface hence capturing the interface shape by calculating this variable in the flow field. The advantage of the VOF method to interface fitting methods is that it can simulate more complex geometries in regions with wave breakdown, without grid regeneration (see Wackers et al. [2009], Hirt and Nichols [1981]). Although using this method does not provide a sharp water-air interface, the solution renders adequate flow field information. The wide region of phase mixture layer is generated using this method especially in re-attachment region (reported also by Matveev et al. [2009]) which can be reduced by locally higher mesh resolution. The volume fraction parameter was selected with the implicit body force formulation.

The two-equation viscous model, SST $k-\Omega$, with low Reynolds correction, was used for turbulence closure. To resolve the wall effect, approximately 20 cells were placed in the boundary layer region close to walls. The enhanced wall treatment is implemented in $k-\Omega$ turbulence closure which makes it less sensitive to y^+ value of the near wall cells. Because the y^+ varies at

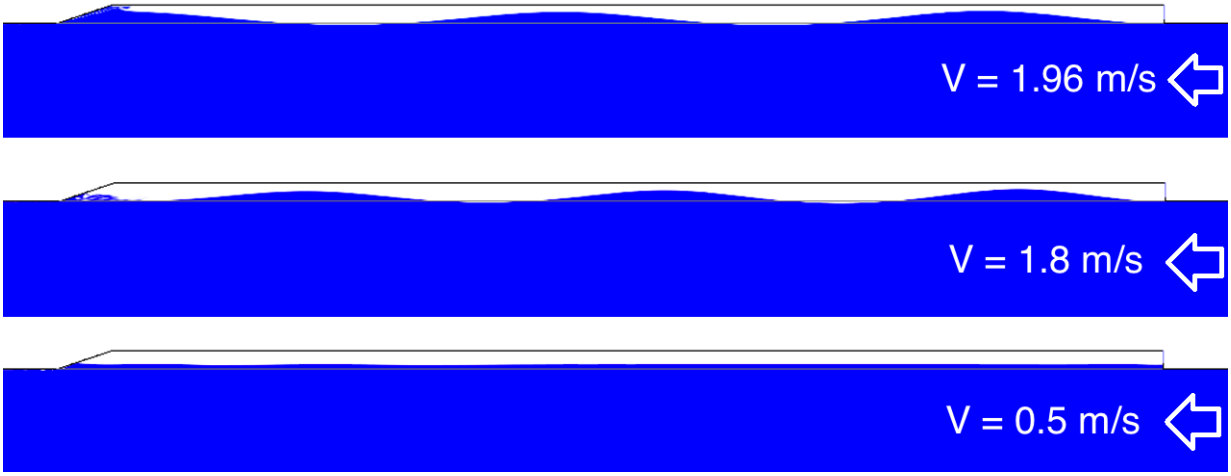

Figure 16: The water-air interface shape inside the cavity in different flow speed. The blue color represents water phase and white color represents air phase.

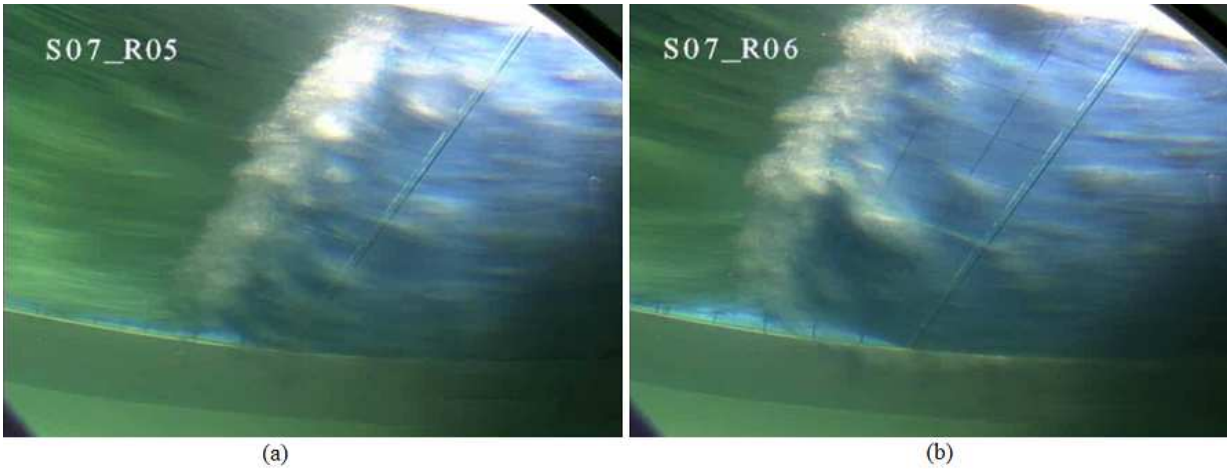

Figure 17: The re-attachment position in different flow speed, (a) U=1.96m/s and (b) U=1.88m/s. The cavity depth for both case is 22cm, slope is 1:5 and cavity pressure is -200pa.

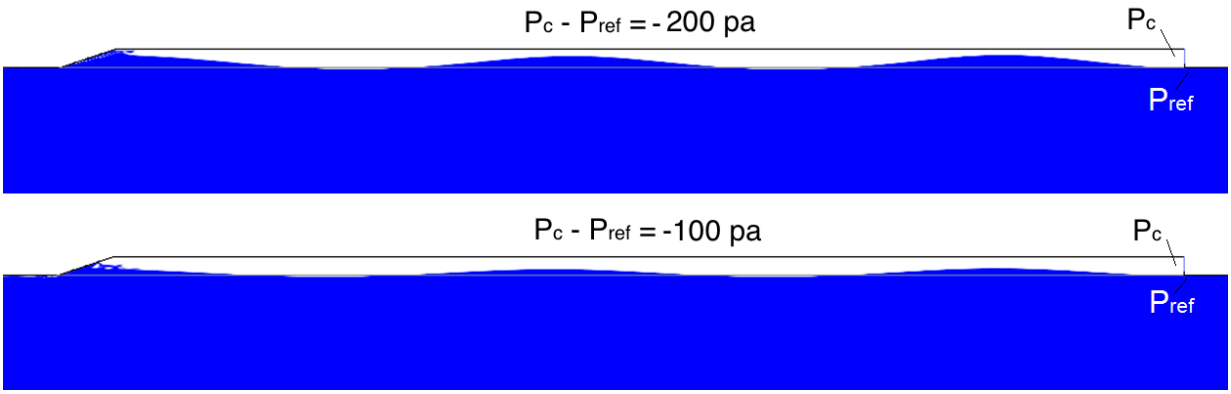

Figure 18: The water-air interface shape inside the cavity with different cavity pressure difference. The blue color represents water phase and white color represents air phase.

the beach region, the choice of adaptive model is necessary to decrease the error for the near wall estimation. The cells adjacent to the beach have an average of y^+ between 1 to 3. This value varies due to unsteady flow condition of the re-attachment region.

The boundary condition and initial condition of the flow field should be selected in a way that even in a stationary condition (zero flow speed) the hydrostatic pressure of the entire domain remains in equilibrium. The initial volume fraction of the field is divided into two region of air inside the cavity and water inside the rest of the test section. The initial water height is then equal to the static submersion of the cavity:

$$\Delta P = \rho_w \, g \, T \tag{4}$$

where ΔP is the pressure difference of the cavity and reference pressure and T is the initial water height from the reference pressure position (cavity's step edge). Since the hydrostatic pressure of the entire cavitation tunnel remains constant (except for the small change due to the wavy air-water interface), the outlet condition is defined as pressure outlet and the *Open Channel Flow* option with the free surface level equal to the static submersion depth (T). The bottom level is the test section's depth. For the air inlet condition, the constant air pressure was set to zero, since the initial condition and the outlet condition dictate the pressure distribution in the field. The upstream water inlet was set to velocity inlet condition with uniform velocity profile.

All walls were considered as hydraulically smooth walls with no-slip boundary condition. The wall adhesion was set with the contact angle between water and air equal to 60 degree and surface tension coefficient equal to 0.072 N/m. The sensitivity of the solution to the surface tension coefficient was not quantitatively studied but the overall behaviour of re-attachment was not sensitive to different values.

The first order implicit temporal discretization was used for transient solver and the PISO scheme was used for pressure-velocity coupling of the discretized RANS equations. The pressure is discretized by *Body Force Weighted* scheme and volume fraction by *compressive* method. For the momentum, first-order upwind scheme was used in the beginning to help the solution's convergence. After the initial phase of the computation, both momentum and turbulence switched to second-order upwind scheme. The time step size was initially set to 10^{-6} s and was increased to 10^{-4} s. Bigger time step than 10^{-4} s could not resolve the detail of the unsteady flow field. *Non-iterative time advancement* was used to compensate for the long time of the computation. The NITA scheme increases the speed and efficiency of the calculation in the high quality meshes. Volumetric flow rate of the inlet air was monitored until it reached a more or less stable condition.

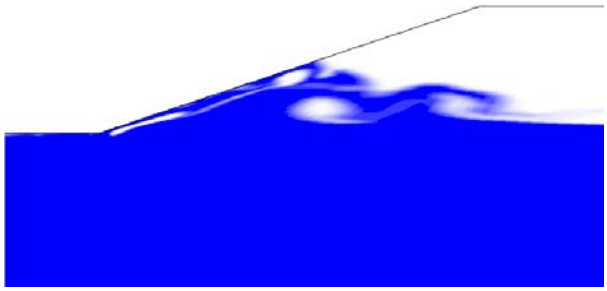

Figure 19: The two-dimensional simulation of the flow field in the beach region. The bubbles are visible in this picture. Blue color represents water phase and white color represents air phase.

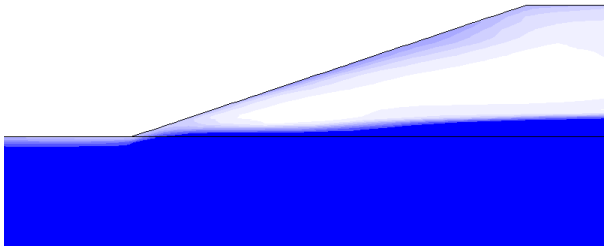

Figure 20: The simulation of the flow field in the beach region with coarse mesh. The layer of air is released from the cavity. Blue color represents water phase and white color represents air phase.

Three computations with the water velocities of U=1.96m/s, U=1.8m/s and U=0.5m/s were performed in the 2-D cavity with depth of 10cm and beach slope of 1:3. The cavity pressure for all three cases is $\Delta P = -200pa$. Figure 16 shows the difference between the wave shape and wavelength of the interface with the same cavity pressure. The free surface at low velocity show very little wavy behaviour and the water re-attachment at beach is smooth and without air release. This is compatible with the observation in the experiment which showed the same behaviour at low speed. The wave amplitude does not differ much between two velocities of 1.96m/s and 1.8m/s, instead the wavelength changes. As expected the considerable change in wavelength for a small change in velocity (8%) is due to the fact that wavelength varies with square of the incoming disturbance velocity ($\lambda = 2\pi U^2/g$). Figure 17 shows the re-attachment position for the cases with the same condition and different flow speeds. The position of the re-attachment on the beach varies with the slight change in the flow speed similar to the simulations.

For the flow speed of U=1.96 m/s, the flow field was computed in two different cavity pressure: $\Delta P = -100$pa and $\Delta P = -200$pa. The negative pressure difference represents the lower cavity pressure compared to the reference pressure, which is equal to the hydrostatic pressure of the water under the hull. The positive pressure results in air release without a stable condition inside the cavity. Neither in experiment nor in computation could create stable condition even with zero pressure difference. Increasing the pressure resulted in more air release up to the point that the air supplier could not deliver sufficient air. In this situation, maintaining the cavity pressure was exacerbated by the unsteady nature of air escape.

2-D Result Discussion

As expected, the free-surface wave amplitude increases by lowering the cavity pressure and the wetted surface decrease by increasing the air pressure inside the cavity. The wavelength does not change but the re-attachment position on the beach slightly differs with the wave amplitude. Figure 19 shows a snap shot of the flow at the beach. The process of bubble making is of course unsteady but when the wave formation reaches to a stable shape, the air release flow rate fluctuates within small range and the average converges to a constant value.

The area of the wetted surface and the beach angle are the parameters which determine the force on the beach plate. The re-attachment position of water on the beach plate provides an estimation of the pressure force on the beach plate. Since the re-attachment position is sensitive to the flow speed, in a similar cavity pressure, the drag force considerably changes when the flow speed slightly varies. Therefore the prediction of the drag force due to re-attachment process is difficult.

The re-attachment and bubble making process were sensitive to the mesh size at the beach region. The VOF method could not resolve the detail of bubbles unless the proper size of the mesh is chosen inside the flow field. The effect of using a coarser mesh is shown in Figure 20. In this figure the a layer of air-water mixture is simulated at the beach and is released under the aft plate. The observation at the experiment suggests the bubbles are in order of few millimetres. The mesh size in the coarse mesh grew up to few centimetres inside the cavity. The refinement of the beach region decreased the size of the mesh close to the proper value. In both cases the near-wall cells were small with the appropriate y^+ value. The bubble making process in refined mesh is similar to the experiment.

Table 2: Number of quadrilateral cells in the grid refinement verification cases.

Case	Number of cells	h/h_1	Air flow rate (lit/s)
Fine mesh 2	789,655	1.0	0.734
Fine mesh 1	445,965	1.33	1.05
Base mesh	210,000	1.94	1.24
Coarse mesh 1	99,963	2.81	1.41
Coarse mesh 2	51,473	3.92	2.0

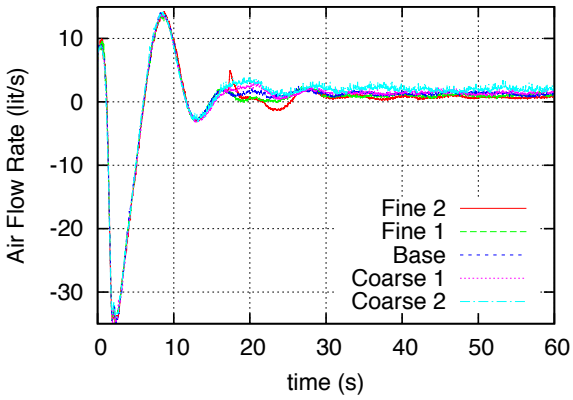

Figure 21: Air flow rate in cases with different mesh resolution.

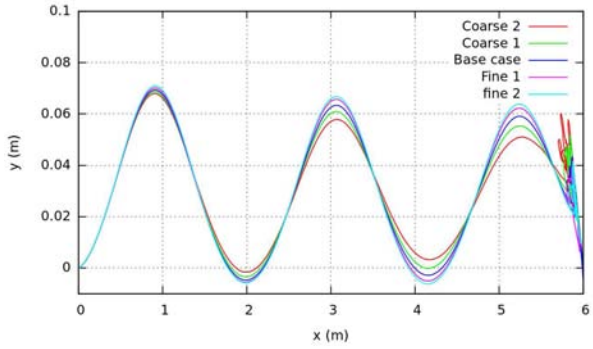

Figure 22: Free surface inside the air cavity in different mesh resolution.

VERIFICATION OF 2-D SIMULATION

Any numerical simulation contains the code and solution uncertainties. The code verification is not the concern of this study since the CFD code that is used here (ANSYS Fluent) has been evaluated for the errors using known benchmark solution. The numerical simulation in a particular solution consists of the grid discretization as the main source of error , therefore we have performed a grid convergence study for solution verification.

In theory the error due to spatial resolution decreases by reducing the size of the grid cells. Five geometrically similar grids are used with different resolution. All the cases have beach slope of 1:3, cavity height of 100 mm, water velocity of 1.9 m/s and cavity pressure of -200 pa. Compared to the base case with 210,000 quadrilateral cells, the grids are made finer and coarser in four other cases. The number of cells for each case and grid refinement ratios are presented in table 2. The first cell size is kept constant in all five grids to avoid the uncertainty due to sensitivity of viscous model to the wall adjacent cell distance.

The air flow rate through the inlet is compared in five different cases and presented in Figure 21. The duration of the simulation is long enough to allow the fluctuating values converge to a constant average and the free surface position remains unchanged. The average air flow rate for the last 10 seconds of the simulation is given in table 2.

Comparing the free surface position inside the cavity shows a cumulative change based on the grid size. Figure 22 shows that this difference is maximum in the last peak and causes a shift in the position of re-attachment on the beach surface. The position and the angle of re-attachment dictate the pressure force on the beach and the air flow rate. The proper verification study for resistance coefficient is difficult since the change in the re-attachment positioning alters the flow field after the beach.

3-D SIMULATION

Three-dimensional model was consist of approximately 2 million hexahedral structured mesh. To decrease the number of cells in the calculation, a symmetry boundary condition is used in the middle of the flow field. The setting of the 3-D computation was similar to the 2-D cases. Figure 23 shows the three dimensional flow field simulation of the free surface. The cavity pressure for this case is -200pa and the beach slope is 1:3. The free surface prediction in 3-D simulation is similar to the corresponding experimental case. The side walls of the cavity create the 3-D shape of the free surface which

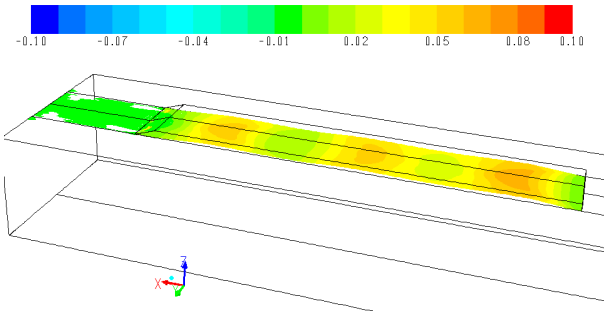

Figure 23: Three dimensional simulation of the flow field. The iso-surface of the volume fraction is plotted and is coloured based on the free surface height. The 3-D wave peaks are similar to the experimental case.

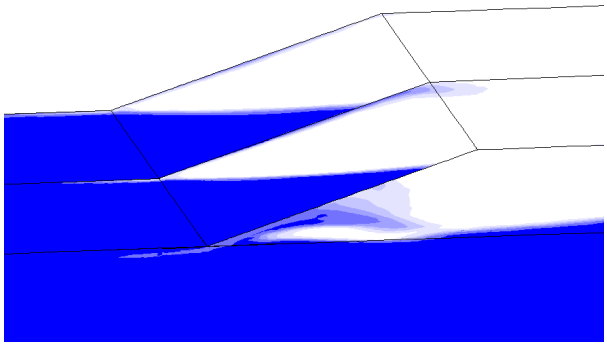

Figure 24: The three-dimensional simulation of the flow field in the beach region. Blue color represents water phase and white color represents air phase. Three stream-wise slices in different locations of the flow field visualize the flow.

shows that 2-D simulation does not provide the proper information for this flow. The experimental results confirm the concave shape of the wave at the center-line of the cavity. The wave amplitude decays toward the cavity rear, but does not fade away.

The re-attachment of the water on the beach plate is shown in the figure 24. To visualize the flow field in the beach region, three stream-wise slices in different locations of the flow field is plotted in one time step of the simulation. Figure is coloured by the phase and blue color represents water phase and white color represents air phase. Forces acting on different part of the cavity in this time step is presented in Table 2 for this case. The force on the beach contributes the most in the total forces acting on the cavity box. The average force for the same case according to Figure 12 is 19.7N on the cavity box and 7.2N on the aft plate. The difference on the aft plate could be because of the air lubrication in the CFD simulation. More resolution on the beach area is required in order to resolve the bubble making process.

To compare the wave amplitude in the experiment

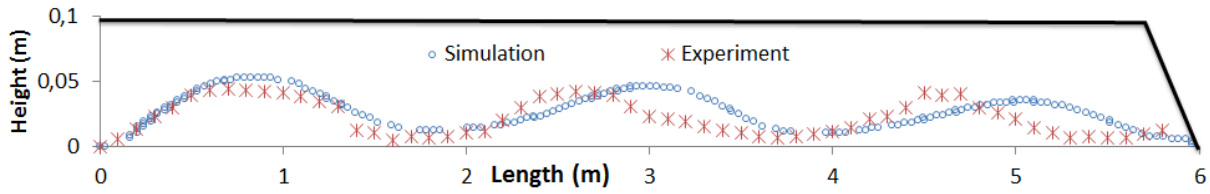

Figure 25: The comparison between the water line on the side of the cavity experiment and simulation.

Table 3: Horizontal viscous forces corresponding to the case shown in Figure 23. The pressure forces and the vertical forces on the beach section is not included.

Section	Force (N)
Beach wall	18.6
Cavity roof	0.3
Cavity walls	2.1
Cavity total	21
Fore plate	14.4
aft plate	3.8

with the CFD simulation, the position of the free surface on the side wall of the cavity which is photographed through the side windows is presented with the same computational case. Figure 25 shows this comparison. The amplitude of the waves are similar but the phase of the waves differs. This difference is cumulative for each period and could be due to the velocity measurement error in the experiment. The exact re-attachment position of the water on the beach varies in both experiment and simulation which makes it difficult to compare the wave height in beach region. Visibility is decreased in the beach photographs due to bubble making process, but in general the position of the re-attachment in the 3-D simulation (unlike 2-D simulation) was lower than the experiment. More 3-D simulations with higher beach resolution are needed to resolve these discrepancies.

Concluding Remarks

Experiment on single cavity showed that a relatively stable free-surface wave is possible to achieve, given a combination of flow speed and cavity air pressure. Even though in some cases the water came in contact with the cavity ceiling, because of the three-dimensional shape of the wave, the integrity of the cavity was maintained and cavity did not collapse.

It was very difficult to run with case of zero pressure difference in the cavity, in fact the air supply controller could not keep up with sudden changes due to release of considerable amount of air in this case. The same scenario can be correct if the cavity move from horizontal positioning due to manoeuvring.

The wetted surface on the side walls of the cavity increased by lowering the cavity pressure, hence the viscous drag force on the cavity increased.

Even though the cavity pressure influenced the amplitude of the wave inside the cavity, the position of the re-attached water on the beach was sensitive to the water velocity. The re-attachment position was affecting the total drag on both viscous and pressure drag at the beach plate. The pressure component of the beach drag was considerably larger than the viscous component. A decrease in beach angle results in larger wetted area on the beach but decreases pressure component of the re-attachment drag. The rate of change in the beach drag was higher when the angle decreased from 1:3 slope to 1:5. This change was much less between the slope 1:5 and 1:7.

The bubbles that were produced from the re-attachment process at the beach were responsible for the air release in the stable cavity (see Figure 17). Although the air bubbles convected from beach toward the aft plate, the drag force on aft plate did not show any decrease. The observation showed that the bubbles were convected away from the aft section and did not help the drag reduction process.

The 2-D and 3-D simulations showed that refinement of the mesh is important to capture the detail of the re-attachment process. In order to compute the forces acting on the beach plate, the detail of the free surface collision into the rear section of the cavity is necessary.

Acknowledgements

The study is supported by Stena Rederi AB and the Swedish Energy Agency, grant 34047-1. The authors would like to thank the technical staff in SSPA AB cavitation tunnel for their support. The computations were performed on resources provided by the Swedish National Infrastructure for Computing (SNIC) at C3SE.

REFERENCES

Foeth, E.J. "Decreasing frictional resistance by air lubrication," Proceedings of the 21th International Hisawa Symposium on Yacht Design and Yacht Construction, 2010.

Hirt, C.W. and Nichols, B.D. "Volume of fluid (VOF) method for the dynamics of free boundaries," Journal of Computational Physics, Vol. 39, No. 1, 1981, pp. 201–225.

İnsel, M., Gökçay, S. and Helvacioğlu Ş. "Air Lubrication for Low Speed Ships," Proceedings of the 13th Congress of International Maritime Association of Mediterranean, İstanbul, Turkey, 12–15 Oct. 2009.

Jang, J., Ahn, I., and Kim, H., "Resistance Reduction of a Small High-Speed Boat by Air Lubrication," Proceedings of the 2nd International Symposium on Seawater Drag Reduction, Busan, Korea, 23-26 May 2005.

Leer-Andersen, M. and , Larsson L. "An experimental/numerical approach for evaluating skin friction on full-scale ships with surface roughness," Journal of Marine Science and Technology, Vol. 8, No. 1, 2003, pp. 26–36.

Larsson, L. and Raven, H.C.,"The Principles of Naval Architecture Series," Ship Resistance and Flow , The Society of Naval Architects and Marine Engineers, 2010.

Lay, K.A., Yakushiji, R., Makiharju, S., Perlin, M., and Ceccio, S.L., "Partial cavity drag reduction at high reynolds numbers," Journal of Ship Research, Vol. 54, No. 2, 2010, pp. 109–119.

Matveev, K.I., "On the limiting parameters of artificial cavitation," Ocean Engineering, Vol. 30, No. 9, 2003, pp. 1179–1190.

Matveev, K.I., "Air Cavity Ships Are Ready for a Wider Market," Speed at Sea, Feb., 2003, pp. 13–16.

Matveev, K.I., "Three-dimensional wave patterns in long air cavities on a horizontal plane," Ocean Engineering, Vol. 34, No. 13, 2007, pp. 1882–1891.

Matveev, K.I., Burnett, T.J., and Ockfen, A.E., "Study of air-ventilated cavity under model hull on water surface," Ocean Engineering, Vol. 36, No. 12-13, 2009, pp. 930–940.

Schlichting, H., Boundary-layer theory, McGraw-Hill, 1979.

Thill, C., Toxopeus, S., and van Walree, F., "Project Energy-Saving Air-Lubricated Ships (PELS)," Proceedings of the 2nd International Symposium on Seawater Drag Reduction, Busan, Korea, 23-26 May 2005.

Wackers, J., Koren, B., Raven, H., Ploeg, A., Starke, A., Deng, G., Queutey, P., Visonneau, M., Hino, T., Ohashi, K. "Free-Surface Viscous Flow Solution Methods for Ship Hydrodynamics," Archives of Computational Methods in Engineering, Vol. 18, No. 1, 2011, pp. 1–41.